University of Zurich[UZH]

Understanding the snow depth distribution in Alpine terrain using random forests

GEO 510 Master's Thesis

Author
Elena Julia Köpfli
17-729-088

Supervised by
Dr. Hendrik Wulf
Dr. Yves Bühler (buehler@slf.ch)

Faculty representative
Prof. Dr. Alexander Damm

30.01.2023
Department of Geography, University of Zurich

University of Zurich[UZH]

GEO 510
Master Thesis
31 January, 2023

Understanding the snow depth distribution in Alpine terrain using random forests

Elena Köpfli
17-729-088

Supervised by:
Dr. Hendrik Wulf
Dr. Yves Bühler

Faculty representative:
Prof. Dr. Alexander Damm

Remote Sensing Laboratories
Department of Geography
University of Zurich

Abstract

The spatial distribution of snow depths is crucial for addressing various scientific questions in Alpine regions. Information on snow distribution helps to better manage water resources and risks such as snow avalanches or flooding. Snow depth in Switzerland is measured continuously in a network of selected automatic weather stations. In this thesis a Random Forest (RF) algorithm is used to model the snow distribution in the Davos region at different spatial scales. The importance of input parameters such as interpolated snow depth measurements, satellite-based information average snow cover and topographic variables is investigated. The RF-model is trained and validated with drone- and aircraft-based snow depth maps. Variables that provide direct information about the distribution of snow, such as snow cover duration (SCD) or interpolated snow depths from gauging stations, are preferred over topographic variables (elevation, aspect, slope, Topographic Position Index (TPI) and Diurnal Anisotropic Heat (DAH)). To investigate the effect of spatial resolution on RF-model accuracy, different resolutions from 6 m to 100 m were tested. Validation of the RF-model reveals that model accuracy increases with decreasing spatial resolution. The average coefficient of determination (R^2) at 6 m and 100 m resolution, being 0.41 and 0.56. In addition, we analyzed the performance of the RF-model on inter-annual and intra-annual time scales. Inter-annual comparison of the snow distribution from the peak of the snow season (in March or April) yields high model accuracy due to similar spatial distribution patterns of snow depth tied to topography. In contrast, an intra-annual comparison results in lower model accuracy due to repeated redistributions during the build-up phase of the snowpack. To test the general validity of the RF-model, we validated the snow model in different regions of Switzerland. The accuracy of the the RF-model varies between a R^2 of 0.28 and 0.51 depending on the test region. Similar topographic characteristics of the training and validation region lead to more accurate model results of the snow distribution. The RF approach chosen in this thesis makes a valuable contribution to improved snow distribution modeling. Future area-wide measurements of the evolution of snowpack can contribute significantly to a better understanding and modeling on the intra-annual snow distribution.

Contents

Abbreviations

DAH	Diurnal Anisotropic Heat
DEM	Digital Elevation Model
DGNSS	Differential Global Navigation Satellite System
DTM	Digital Terrain Model
HS	Height of Snowpack
IMIS	Interkantonales Mess- und Informations-System
KDE	Kernel Density Estimation
k-fold CV	k-fold Cross Validation
LiDAR	Light Detection And Ranging
MAD	Median Absolute Deviation
MAE	Mean Absolute Error
ML	Machine Learning
RF	Random Forest
RLS	Regression Line Slope
RMSE	Root Mean Square Error
R^2	coefficient of determination
SCD	Snow Cover Duration
SWE	Snow Water Equivalent
TIN	Triangulates Irregular Network
TLS	Terrestrial Laser Scanning
TPI	Topographic Position Index
UAS	Unmanned Aerial System
VTOL	Vertical Take-Off and Landing

List of Figures

List of Tables

1 Introduction

1.1 Relevance of snow

Snow is an important freshwater reservoir in mountain areas (Viviroli et al., 2007). The population, agriculture and electricity industry around snow-rich areas depend on clean melt-water which is used for drinking, irrigation or for hydro-power electricity (Farinotti et al., 2012). Large amounts of melt-water within a short time can cause flooding (Di Marco et al., 2021). Beside flooding, snow avalanches are another natural hazard strongly influenced by snow distribution. Especially in populated mountain areas like the Swiss Alps, it is important to monitor the current danger of avalanches. Avalanches depend on the absolute amount of snow as well as the snow distribution (Bühler et al., 2015; Schweizer et al., 2003) and the water stored in the snow (Snow Water Equivalent SWE) (Jonas et al., 2009).

1.2 Snow depth mapping

Snow depth or height of snowpack (HS), defined as the vertical distance from the base to the surface of the snowpack (Fierz et al., 2009), can be measured with two different approaches: specific points or area wide measurements (Eberhard et al., 2021; Bühler et al., 2021). Point measurements can be done manually or by automatic weather stations. In many mountain regions a network of automatic snow measuring stations is maintained (Winstral et al., 2019; Vionnet et al., 2016; Serreze et al., 1999). Other automatic point measurement techniques are snow pillows (Archer and Stewart, 1995) and sonic distance sensors (Senese et al., 2014). Snow pillows measure the SWE automatically based on the weight of the snow cover per area. Sonic distance sensors (Senese et al., 2014) release ultrasonic pulses and measure the snow depth based on the travel time difference. Such automated point measurements have been employed successfully for many years. Area-wide manual measurements are done with ground-penetration radar (GPR) (McGrath et al., 2019). But manual data collection involves entering technically challenging terrain, which is often highly susceptible to avalanches. Therefore, the data set often includes several data gaps in regions of interest. To fill these gaps, more automated field measurement techniques as for example Magnaprobe (Sturm and Holmgren, 2018) are used. Modeling is successful to get from discrete point data to the area wide scale (Nolan et al., 2015; Liston et al., 2007; Serreze et al., 1999). Especially in high Alpine regions where the snow distribution is irregular, point measurements are not sufficient to assess the avalanche danger because of strong local snow depth variations.

To account for these shortcomings, remote sensing techniques allow for area-wide coverage of snow depth measurements including inaccessible terrain (Bühler et al., 2015). Airborne LiDAR is a successful tool for mapping snow depths (Nolan et al., 2015). Inaccuracies in the snow depths occur especially on steep slopes. These inaccuracies occur due to horizontal localization inaccuracies of the airborne LiDAR system (Nolan et al., 2015; Schirmer et al., 2011). Terrestrial laser scanning (TLS) measure the snow height with a accuracy below 10 cm, but are not appropriate by covering larger areas (Mendoza et al., 2020). Passive photogrammetric snow depth mapping can be done satellite-based, airplane-based, unmanned aerial system (UAS)-based and from terrestrial imagery. The different heights of the platforms have advantages and disadvantages in spatial and temporal resolution as well as measurement accuracy (Eberhard et al., 2021). Modeling combines the fine temporal resolution of the measurement stations with the area-wide measurement data of the RS-systems. Adapted to the final application, a snow depth map can be modeled at the desired temporal and spatial resolution.

1.3 Snow depth modeling

The snow depth in mountain areas has large spatial heterogeneity, which is mainly driven by the complex interactions between low atmospheric levels and local topography (Sturm and Holmgren, 2018; Sturm and Wagner, 2010; Trujillo et al., 2009). Despite substantial effort by the scientific community to determine the spatial scale at which the various processes act, a number of snow processes directly related to terrain characteristics are not fully understood. Several statistical methods have commonly been used to determine the relationship between snowpack distribution and topographic variables. These include linear regression models (Zheng et al., 2016; Fassnacht et al., 2003), multiple linear regression models (Grünewald et al., 2013), binary regression trees (Gleason et al., 2017), and general additive models (Sturm and Wagner, 2010). More recently, random forests gained attention by accurately modeling snow depth distributions in different alpine environments, while providing an improved understanding of the underlying snow distribution processes (Revuelto et al., 2020; Cartwright et al., 2022; Nasim et al., 2022).

The snow models already developed use different input variables (Revuelto et al., 2020; Cartwright et al., 2022; Grünewald et al., 2013; López-Moreno et al., 2017; Daudt et al., 2022). The relation between elevation and snow depth has already been studied by Grünewald et al., 2014 and is usually integrated into snow depth models. Based on the composition and operation of the model, the parameter weighting can vary greatly. The large variety of variables in existing snow depth models shows that the influence of the variables on the snow models has not yet been fully understood. The validation data and their spatial coverage often determine the spatial resolution. Grünewald et al., 2013; Revuelto et al., 2014 shows the tendency of more

precise snow depth models with increasing pixel size. Revuelto et al., 2020, Daudt et al., 2022, Cartwright et al., 2022 and López-Moreno et al., 2017 model with a more detailed spatial resolution in the meter range in contrast to Grünewald et al., 2013 who gains his insights with pixel sizes from 100 m to 800 m. But generally, the influence of spatial resolution has been barely discussed. The time dependency of the training and validation data has hardly been considered so far. This requires validation data at different points in time. Training times are selected based on available data in the developed snow models. The effect of the timing in a snow season of the training data on model accuracy has not been sufficiently considered in previous studies. The application of the snow model in an arbitrary region is a goal of the snow depth model. Grünewald et al., 2013 and Revuelto et al., 2020 show difficulties of snow distribution for regions which were not integrated in the training set. The application areas of snow depth maps, such as the assessment of avalanche danger, require snow depth models that are as flexible as possible in terms of time and space.

1.4 Research objectives

In this thesis, I aim to better understand the role of topography on snow depth distribution at different spatial scales. I will analyse the weighting of different topographic variables in explaining the snow depth distribution with random forests in different spatial resolutions and study areas in the Swiss Alps. The adaptability of the model to the variation in snow distribution over the course of a snow season will be tested. This intra-annual analysis will be compared with an inter-annual evaluation, with snow depth maps at a similar time in the snow season but in a different year. Using the larger training region, I optimize the transferability of a snow distribution model. The unique datasets obtained by aerial surveys from the WSL Institute for Snow and Avalanche Research SLF will serve as reference datasets for training and validation in my modeling approach. In this context, I will investigate the following Research Questions (RQ):

- RQ 1: Which parameters are most relevant to model the spatial snow depth distribution?
- RQ 2: Which influence imposes the spatial scale on the modeling accuracy?
- RQ 3: How does inter-annual and intra-annual snow modeling differ?
- RQ 4: To which degree can RF-models be transferred among different alpine locations?

2 Study area

The main study area is located in the eastern part of the Swiss Alps around the village Davos. Due to different data availability, I use multiple study regions (Figure 2.1) to answer the four research questions. In this thesis, the study region Davos serves as the basis for all snow modelings. Other study regions (inset map in Figure 2.1) in the Swiss Alps are included to test the transferability of the trained model.

2.1 Target area Davos

Varying flights routes during image acquisition results in different extents of the derived snow depth maps. Different parts of the big study area in Davos have already been used for other snow mapping studies as: the Weissfluhjoch (Wirz et al., 2011), Jakobshorn (Bühler et al., 2014; Bühler et al., 2016), Latschüelfurgga (Schweizer et al., 2003), the Dischma valley which runs from Davos to the south (Grünewald et al., 2014; Bühler et al., 2015; Eberhard et al., 2021) and the parallel Flüela valley (Bühler et al., 2016).

The Davos area is located in a transit zone between the humid north-alpine climate and the drier central Alps climate (Kulakowski et al., 2011). Many snowfall events are associated with a northwestern or northern orographic lift. Therefore, the snowfall is often combined with a lot of wind. In the Davos area the maximum snow peak is between March an April (Begert et al., 2005). The average snow depth of the study area during the snow peak varies around 1 m to 2.5 m.

The diversity of the terrain includes settlements, heavily forested, vegetation less and glaciated areas. Therefore, the region is representative for many Alpine regions (Kulakowski et al., 2011). Beside the great variety in surface coverage also the terrain diversifies in slope steepness and exposition. Figure 2.2 represents the elevation distribution of all study regions. The main region Davos reaches over 1700 m from 1500 m.a.s.l. to 3200 m.a.s.l. Therefore, the region Davos includes most of the elevations of other study regions (see Figure 2.2). This is the most important altitude zone for observing snow amounts in Alpine region (Grünewald et al., 2014; Laternser and Schneebeli, 2003).

To answer the four research questions, I use different study regions due to the data basis and location. The skin area in which the RF-model is trained is the Davos region (framed in red in Figure 2.1). Additionally model tests at different spatial resolutions and the variable im-

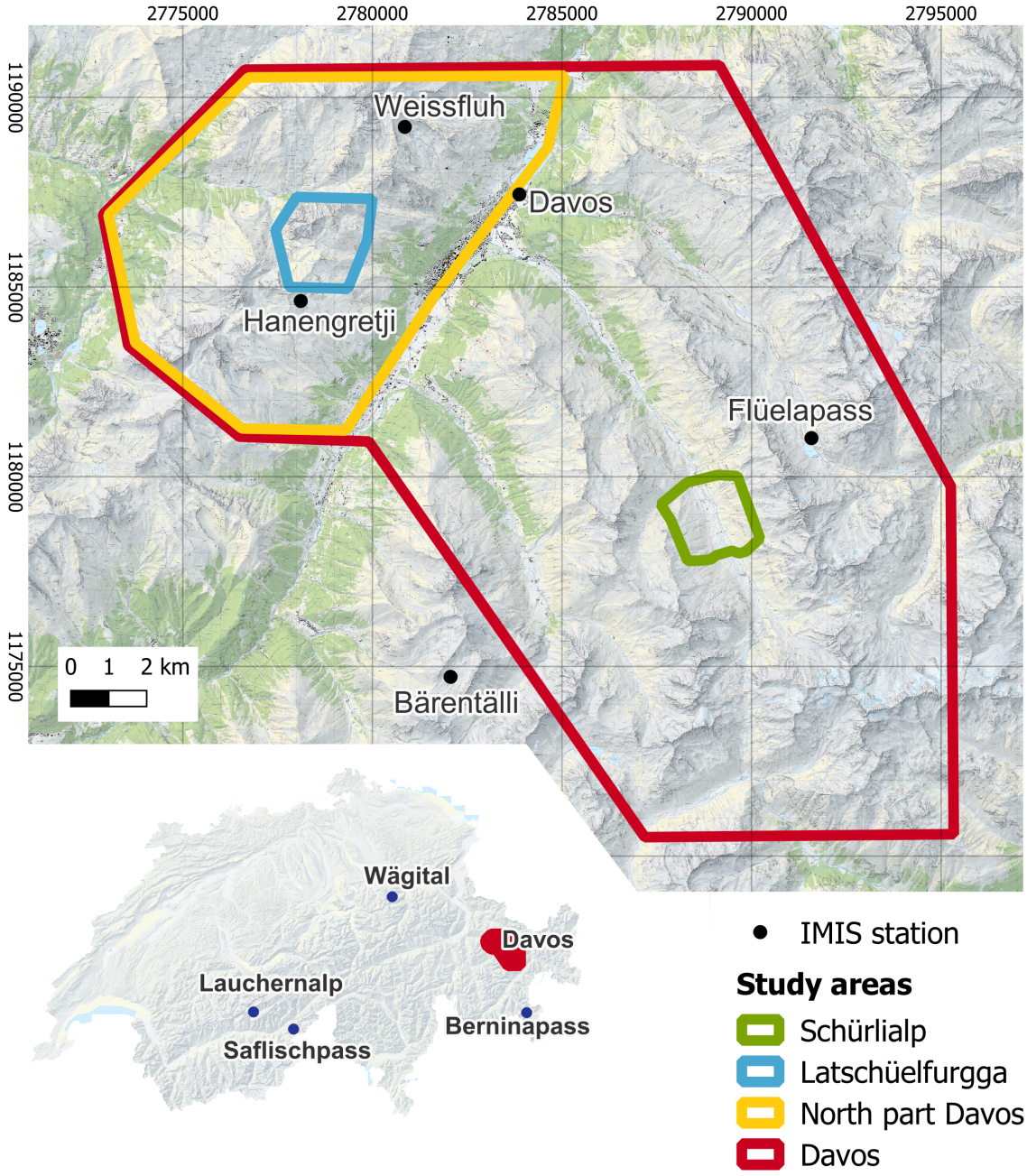

FIGURE 2.1: Overview of the Davos study area with the different study regions of the snow depth surveys and the locations of the IMIS station in the Swisstopo national map (LK25). The inset map on the lower left corner contains the position of the study regions used for extrapolation outside the Davos region as well as the location of the main map.

portance are investigated in the Davos region. For a more detailed consideration of the modeling at different times in a snow season, I use two sub-study areas within the Davos region, Latschüelfurgga (blue in Figure 2.1) and Schürlialp (green in Figure 2.1). Latschüelfurgga and Schürlialp have additional drone-based data at different times throughout a snow season. To test the transferability of the RF-model to other Alpine regions, I use additional study regions distributed over the Alps. In the additional study regions (Saflischpass, Berninapass, Laucher-

enalp and Wägital) the trained model can be tested in other conditions and independently from the test region Davos. As reference, the Davos region is also tested in an extrapolation procedure. For this purpose, the main Davos region (red in Figure 2.1) is divided into a north and a south part of the main valley. The northern part (yellow in Figure 2.1) acts as test region for the model, which is trained in the southern part of the Davos region. Due to the spatial proximity of the training region to the testing region, I check whether the proximity of the test and training regions brings advantages to the RF-model predictions. The different study areas allow to test several time and spatial resolutions as well as the spatial transferability of the model to other alpine regions.

2.2 Validation sites in Switzerland

I test the extrapolation of the RF-model, which is trained in the Davos region, in four other Alpine areas (dark blue dots in the inset map in Figure 2.1). Laucherenalp is located on a southeast slope in the Lötschental in the canton of Valais. The very one-sided exposure with large altitude differences and glaciated patches in this Laucherenalp, covers similar elevations as the training region Davos (Figure 2.2). The barely vegetated Saflischpass includes a topographically diverse region in the canton of Valais. The highest study area is located at the Berninapass. The considered area reaches from Lago Bianco 2234 m.a.s.l., upward into the southwest exposed hillside. The terrain, crossed by the railway line and the pass road, includes a southwestern slope with many couloirs. Of all comparison regions, the Wägital is by far the lowest. It is situated in the canton of Schwyz and the study area stretches from 1200 m.a.s.l. to just below 2000 m.a.s.l. (Figure 2.2) and consists of a heavily forested northwestern slope, while the upper part of the study area is covered with typical prealpine grassland and vegetation-free rocky areas. In order to test the transferability of the model region independently, a part of the study region Davos is separated. The northern part marked in yellow in Figure 2.1 is tested with the RF-model trained in the southern part. These five study areas are intended to show whether the RF-model can accurately model snow depths in regions not used for training.

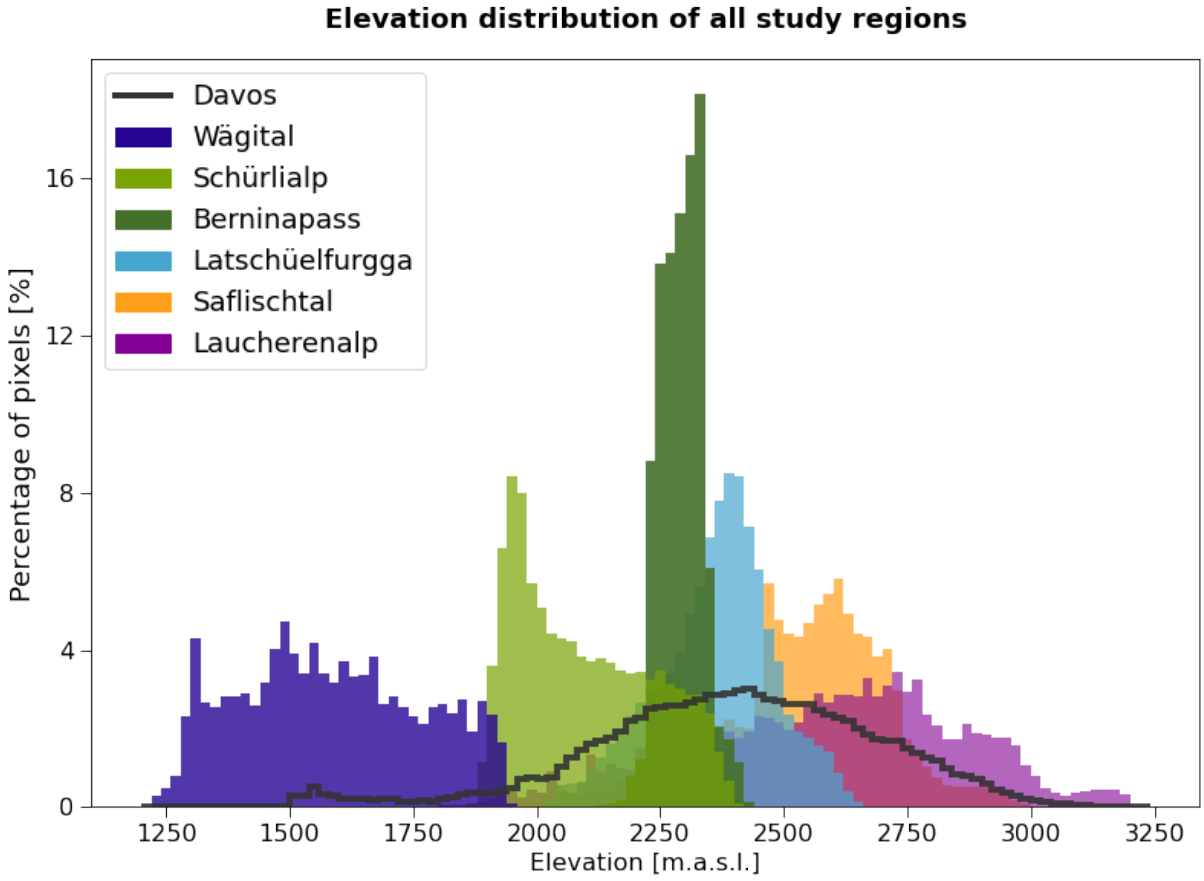

FIGURE 2.2: Elevation distribution of the normalized number of pixels within the individual study regions. This analysis is based on the swissALTI 3D elevation model with a spatial resolution of 10 m. The y-axis shows the number of pixels from each study region in percentage. One bin lasts over 20 m elevation. The colored area represents 100% in each study region.

3 Data

The modeling of snow depths is based on four sets of data: (1) the snow depth maps recorded by photogrammetric combination of aerial photographs, (2) a Digital Elevation Model (DEM) to calculate all topographic variables, (3) the interpolated snow depths from measuring stations (interp. HS) and (4) a satellite-based snow cover duration (SCD). These data sets are described in detail in this chapter.

3.1 Snow depth surveys

To train and validate the snow depth model, I use HS maps from drone and aircraft surveys. All measured snow depth maps are preprocessed from the WSL (Swiss Federal Institute for Forest, Snow and Landscape Research) for Snow and Avalanche Research (SLF) in Davos. The photogrammetric technique is suitable for the processing of an area-wide and precise snow depth map (Bühler et al., 2015; Bühler et al., 2016; Eberhard et al., 2018; Eberhard et al., 2021; Bührle et al., 2022).

3.1.1 Data and sensor

The number of snow depth maps in the different study regions varies considerably. In the main study area Davos, repeated snow depth measurements are available every year. These were carried out area-wide at the respective snow maximum around March or April (Table 3.1). The exact spatial coverage of the resulting snow map changes slightly from year to year (Figure A.5). Since all snow depth maps of the Davos region are based on aircraft overflights, large study regions with detailed spatial resolution between 0.5 m and 2 m are available. In contrast to the annual surveys in the Davos region, there are several overflights within a winter season on Latschüelfurgga and Schürlialp. These drone-based surveys allow for a intra-annual comparison, but no direct inter-annual analysis. Figure 3.1 shows a HS map of the Latschüelfurgga region. In the study areas outside the Davos region: Wägital, Berninapass, Saflischpass and Laucherenalp, one or two drone-based overflights were recorded (detailed overview Table 3.1). Drone-based snow depth maps contain details with high spatial frequency and an spatial resolution of 10 cm. Compared to aircraft-based snow depth maps, drones cover a smaller area. The high precision of the resulting snow amounts is useful for training and validating the snow depth model.

TABLE 3.1: The table includes all snow depth maps used in this thesis. Besides the date and the region, the resolution in pixel size, the covered area and the mean snow depth are noted.

Date	Study region	Resolution [m]	Area [km2]	Mean HS [m]
16.04.2010	Davos GR	2	118.39	2.16
20.03.2012	Davos GR	2	127.13	1.96
15.04.2013	Davos GR	2	125.10	1.56
17.04.2014	Davos GR	2	98.03	1.11
15.04.2015	Davos GR	2	104.77	1.29
26.01.2016	Davos GR	2	104.60	0.72
09.03.2016	Davos GR	2	109.84	1.5
20.04.2016	Davos GR	2	104.51	1.1
16.03.2017	Davos GR	0.5	76.34	0.97
11.04.2018	Davos GR	0.5	24.54	1.35
16.03.2019	Davos GR	0.5	69.73	1.95
06.04.2020	Davos GR	0.5	65.43	1.11
16.04.2021	Davos GR	0.5	145.58	1.63
16.03.2022	Davos GR	0.5	164.92	1.05
06.04.2018	Wägital SZ	0.1	2.45	1.86
02.04.2019	Wägital SZ	0.1	2.45	1.21
23.02.2022	Saflischpass VS	1	6.16	1.98
24.02.2022	Laucherenalp VS	1	3.18	1.15
01.04.2021	Berninapass GR	0.1	2.42	1.45
28.10.2020	Latschüelfurgga GR	0.1	3.40	0.43
18.12.2020	Latschüelfurgga GR	0.1	3.47	0.52
24.02.2021	Latschüelfurgga GR	0.1	3.60	1.33
26.03.2021	Latschüelfurgga GR	0.1	3.49	1.35
09.02.2022	Latschüelfurgga GR	0.1	3.43	1.14
23.02.2018	Schürlialp GR	0.1	3.36	1.48
07.04.2018	Schürlialp GR	0.1	3.38	1.41
18.02.2019	Schürlialp GR	0.1	3.45	1.37
17.12.2020	Schürlialp GR	0.1	3.09	0.39
16.04.2021	Schürlialp GR	0.1	2.83	1.04

All snow depth maps were produced using photogrammetric methods. The aerial photographs were acquired by overflights with an aircraft or with different types of drones. The snow maps in the smaller study areas are based on drone surveys. Drone types range from quatrocopters such as the Phatom4 to the single-rotor eBee to the advanced vertical takeoff and landing (VTOL) WingtraOne (Figure 3.1 b) (Bührle et al., 2022). Reference points are distributed in the study area and measured with Differential Global Navigation Satellite System (DGNSS) (Bühler et al., 2015). This procedure is done as a control in addition to the automatic georeferencing. The larger HS map of Davos, is calculated from aircraft imagery (Appendix A, Figure A.5). Since the technical progress in camera technology are currently developing rapidly, different cameras have been used over the long periods of data release. The first snow depth map used from 2010, was taken with the ADS40/80 optoelectronic scanner. The successor sensor ADS100 was first used in winter 2015. The spatial resolution of the input images with the settings used is 0.25 m for the ADS40/80 and improved to 0.18 m for the AS100. From 2017 since now the Ultracam series (Vexcel Ultracam X and Ultracam Eagle M3) was utilized (Bührle et al., 2022). The more modern survey camera allows aerial photography with a higher spatial resolution of 0.1 - 0.15 m. This improves the spatial resolution of the snow depth map from 2 m to 0.5 m since 2017.

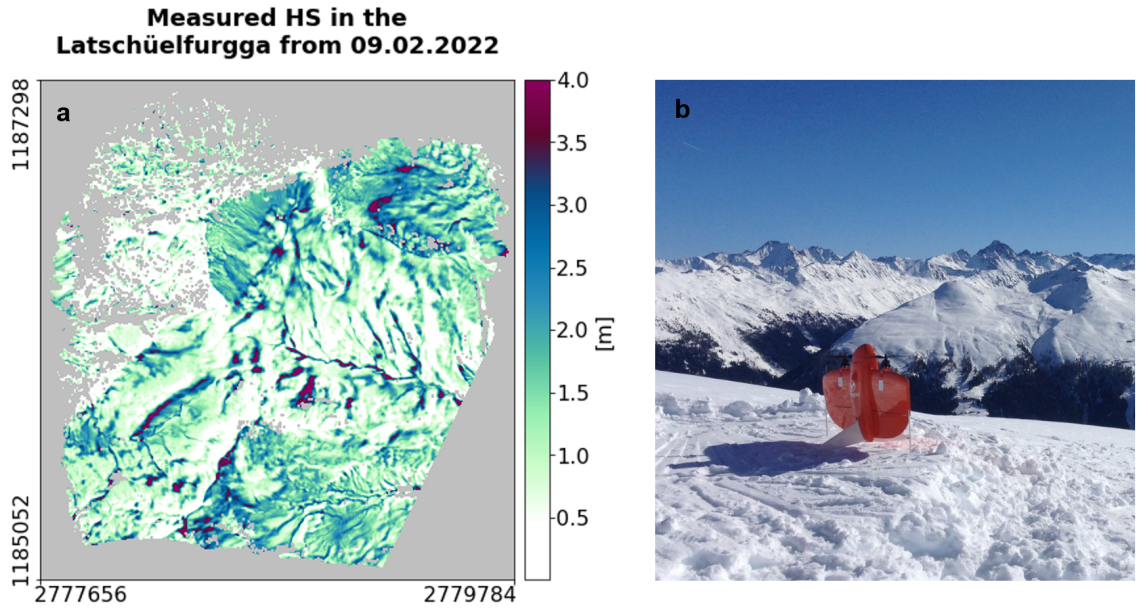

FIGURE 3.1: (a) Snow depth map from Latschüelfurgga. We recorded the basis data with (b) the WingtraOne on February 9, 2022.

3.1.2 Processing snow depth maps

To produce a snow depth map from the individual aerial photographs, many processing steps are required. These are described in detail in Bührle et al., 2022. The Scale Invariant Feature Transform (SIFT) algorithm from Lowe, 2004 transforms image data into scale-invariant coordinates relative to local features. Each individual image is localized and assembled into an area-wide mosaic in the Agisoft Metashape software. Due to the pixel tracking of the software, each pixel is re-localized. The result is a three-dimensional point cloud. Based on the principle of photogrammetry, the distance to the sensor can be measured by taking pictures of the same object from different viewing angles. With the help of the exact sensor positions at each point in time, the Digital Surface Model (DSM) is generated. This DSM contains the topmost point of the surface. Therefore the snow depth is integrated into the DSM. As a comparison to the snow covered surface, a ground truth reference image is generated based on snow free imagery during summer (Marti et al., 2016). To generate the HS map, the DTM is subtracted from the DSM. The difference should then represent the snow depth.

Since this simple principle relies on an undesirable time difference between the two images, additional changes can lead to errors in the results. Therefore, areas with the following landscape coverages are masked out: urban area, summer snow, glaciers, water areas and high vegetation. Outliers in the measured snow depth maps are also masked out. This masking of surface types is necessary because of the time gap between the snow-free ground truth recording and the snow-covered overflight. Due to changes in glacier extent and volume as well as the different water levels of lakes and rivers over time, there is a inconstant snow-free ground truth observation. Therefore, snow amounts on glaciers or frozen lakes cannot be recorded precisely with the photogrammetric technique. In areas with high vegetation, snow depth measuring is very challenging (Gleason et al., 2017). The amounts of snow in vegetation-rich areas are partly distributed on top of and underneath the vegetation. In addition, the strong variation in the DSM is a further difficulty. If small shifts in the georeferencing or other errors can lead to very large or negative snow depths, these are filtered out of the snow depth map. In case of strange structures in the snowdrift map or extreme values, a comparison with the ortofoto or the map can help to understand the generated snow depth maps.

3.2 Digital Terrain Model (DTM)

The Swiss federal office for topography (swisstopo) generates every six years an updated DTM called swissALTI3D. This DTM includes the terrain elevations in 2 m spatial resolution without buildings or vegetation. The product covers Swizerland and the Principality of Liechtenstein and is georeferenced in the Swiss coordinate system CH1903+. The DTM is based on different databases. The base grid below 2000 m.a.s.l. was generated by laser measurement points. Above 2000 m.a.s.l., point values are calculated by means of stereo correlation and specifically

revised photogrammetric. From the point clouds of the laser measurements as well as the stereo correlation and the manually recorded tracking, the desired grid is calculated by means of linear interpolation and triangulated irregular network (TIN). The tracking is done by photogrammetry based on current aerial photographs from swisstopo in a six-year cycle. Due to the different databases and survey methods, swissALTI3D does not have a uniform accuracy. With respect to the fine-meshed 2 m grid, an accuracy of $\pm$ 0.5 - 1 m below 2000 m.a.s.l. and $\pm$ 1 - 3 m above the 2000 m.a.s.l. the limit can be calculated. Manual re-surveys (measuring points, break lines and surfaces) maximize the accuracy to a mean deviation of 0.25 - 1 m.

3.3 Automated measurement stations

The change in snow depths over time can be recorded by automated measuring stations. Snow depth measurements from permanently installed meteorological stations serve as important reference points for the cumulative amount of water stored in snow. In the Swiss Alps and the Jura, snow depths have been systematically recorded since 1996 by the meteorological measuring station network IMIS (Intercantonal Measuring and Information System). Most IMIS stations are located near potential avalanche starting areas. In order to generate an initial estimate of the spatial snow distribution from these point measurements, they were spatially interpolated using the ordinary kriging method. Measured snow depths from neighboring stations in Austria and Italy as well as the DTM were included in the spatial interpolation. This spatial interpolation snow depth distribution was kindly provided by Bernhard Sassik, who already had these data available. The interpolated snow depth distribution serves as the basis for the amount of snow measured at the time of modeling. Since the positional characteristics of the measuring stations are different, the kriging procedure with the DEM is intended to provide an initial estimate of the snow depth distribution and to quantify its change over time. By using many station values, even at greater distances from the study region, extreme values are smoothed. This can be caused, for example, by a strongly wind-exposed location of the measuring station. In addition to snow depths, IMIS stations also provide information on weather conditions prior to the survey of an areal snow depth measurement. These data help in the interpretation of exceptional snow distributions, such as heavy snow drift during storm events.

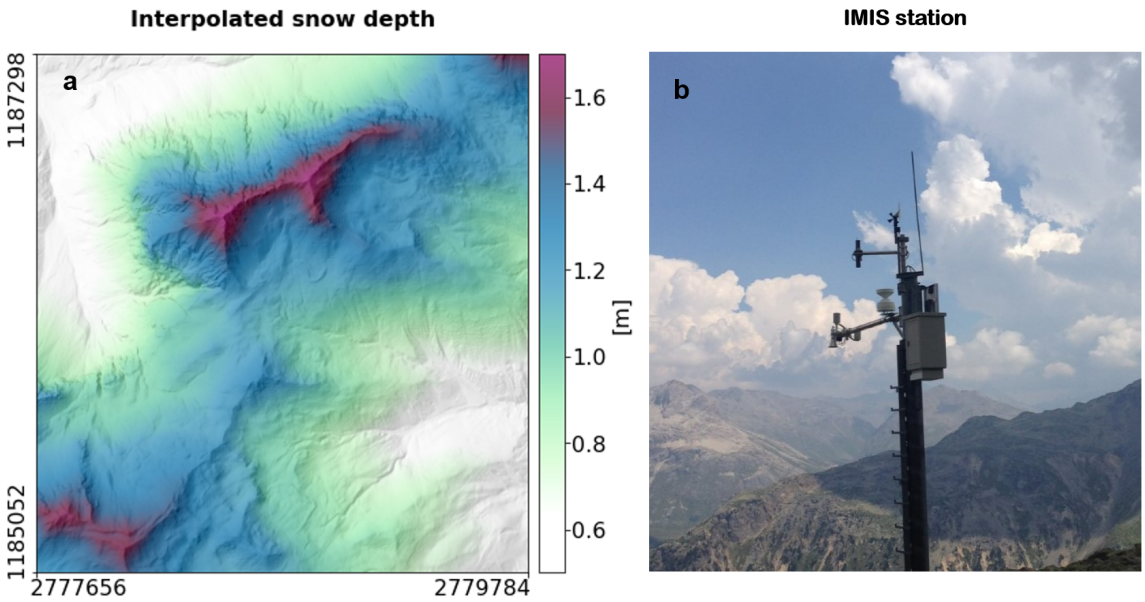

FIGURE 3.2: (a) Interpolated snow depth map with SwissALTI3D hillshade from the Latschüelfurgga study region, based on fixed installed measurement stations (b) IMIS snow-station Puoz Bass on 2625 m.a.s.l.

3.4 Snow Cover Duration (SCD)

Snow cover duration (Figure 3.3) averaged over several years gives a spatial distribution of temporal snow cover patterns. These data are useful for modeling snow depth distributions, assuming that regions with longer snow cover also have higher snow depths. Snow cover duration data in the study area was generated by Hendrik Wulf based on Sentinel-2 data from 2016 to 2021. Here, the Sentinel-2 scenes were binary classified for their snow cover (snow free or snow covered) and cloud covered areas were masked. The large number of images over the six years results in a percentage value of average snow cover per pixel with a spatial resolution of 10 m.

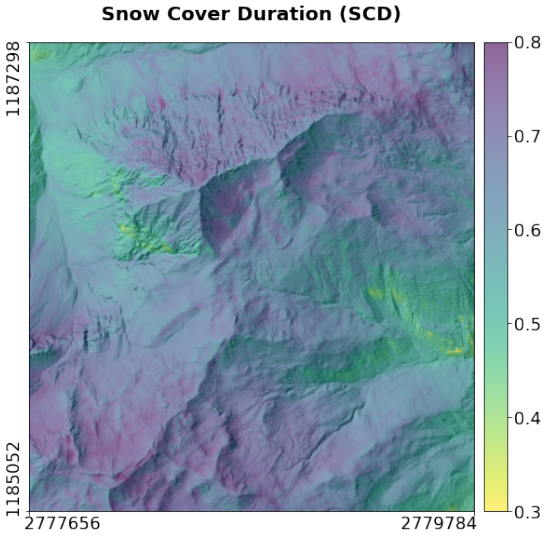

FIGURE 3.3: Proportion of the Snow Cover Duration (SCD) in the Latschüelfurgga region over the hillshade from SwisssALTI3D.

4 Methods

4.1 Overview

In this thesis, a RF-model (Figure 4.1) is used to model snow depths. The RF-model utilizes topographic variables, SCD and the interpolated snow depth to model the snow distribution over a region. Feature Importance (FI) describes the importance of variables in the RF-model. In three data analysis steps, the correlations of the input variables are examined. The model precision is examined using different statistical distribution measures.

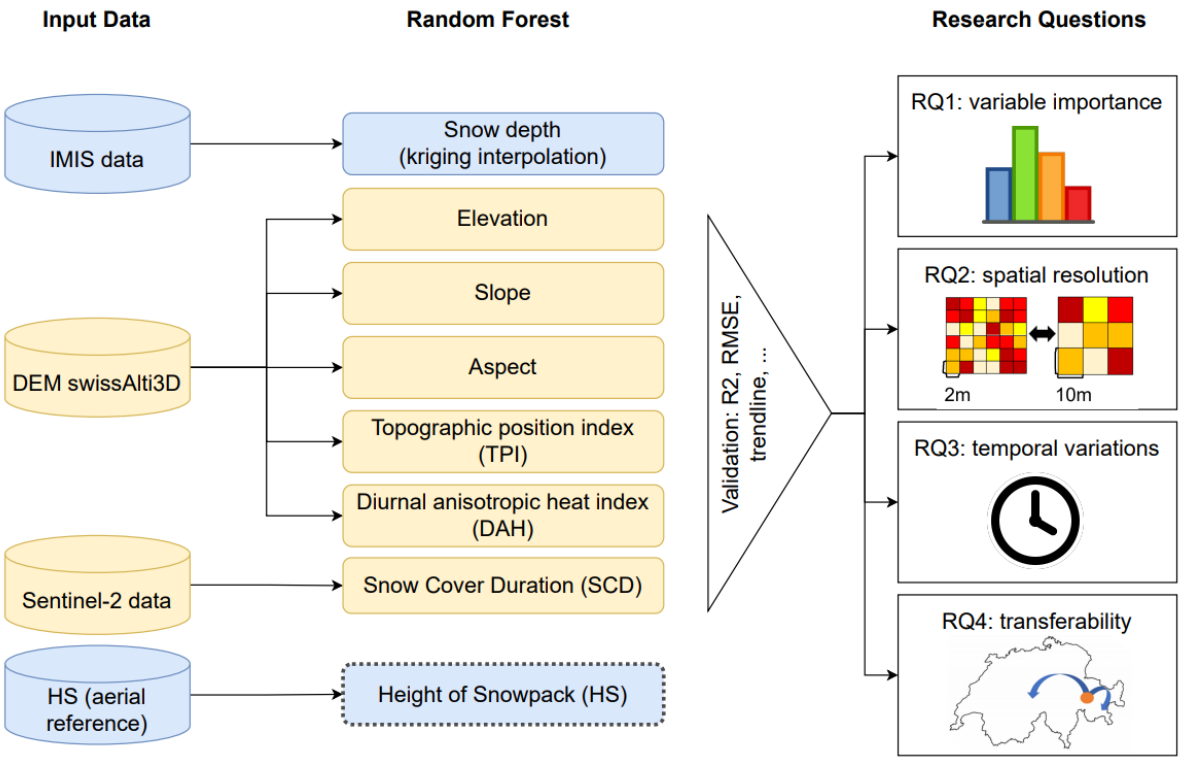

FIGURE 4.1: This flowchart summarizes the working process from input data through the Random Forest-model to answering the four research questions. The yellow fields are not time bounded data or variables. Input data or model variables that are highlighted in blue vary over time. The dotted outline of the model variable highlights the snow depth maps as the resulting variable. This is modeled by the Random Forest but also used in the training procedure. In the right column, the four research questions are shown symbolically.

4.2 Topographic variables

Terrain information is integrated into the RF-model with the elevation, slope, aspect, Topographic Position Index (TPI) and the Diurnal Anisotropic Heat index (DAH) as topographic variables. All topographic variables based on the snow-free DEM from swissAlti3D (swisstopo, 2022) with a spatial resolution of 2 m. The selection of the topographic variables is based on the findings of published studies (Revuelto et al., 2020; Grünewald et al., 2013; Golding, 1974). Slope and aspect are calculated from the DEM using QGIS algorithms from Zevenbergen and Thorne, 1987. The DAH and TPI are calculated in the System for Automated Geoscientific Analyses (SAGA). To analyze the dependence of spatial resolution on model precision, I re-scale the DEM into coarser pixels from 2 m to 6 m, 10 m, 20 m, 50 m and 100 m. The average combines neighborhood cells into one pixel to achieve a coarser spatial resolution. The calculations of the other topographic variables are based on the re-scaled DEM.

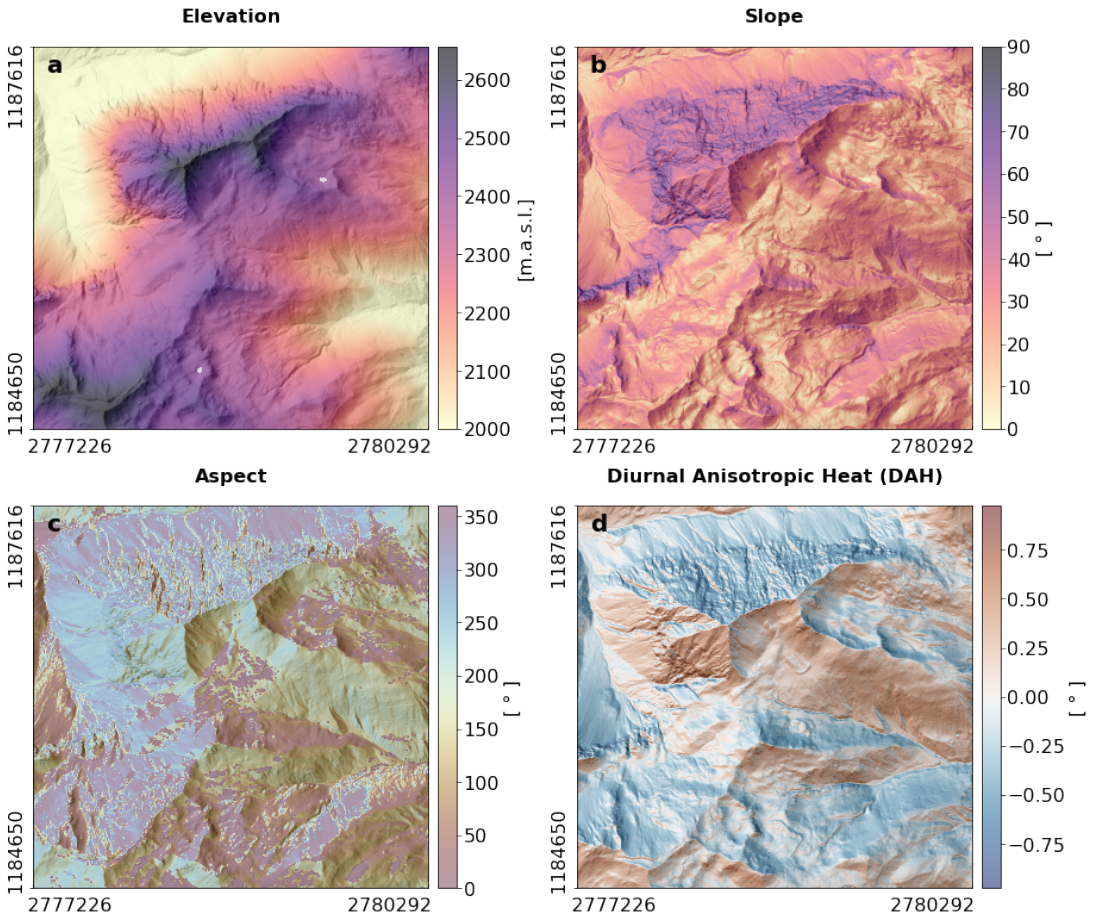

FIGURE 4.2: From the (a) elevation model of the Latschüelfurgga region, the (b) slope, (c) aspect and (d) Diurnal Anisotropic Heat index (DAH) were calculated. These four topographic variables are presented on a hillshade, based on the swissAlti3D.

4.2.1 Diurnal Anisotropic Heat Index (DAH)

The DAH represents a simplified solar irradiance by combining the slope and aspect. The diurnal course of the sun is not considered in the DAH. Incoming solar energy per area is important during the snow melting process. The DAH developed by Böhner and Antonić, 2009 uses the maximum total heat surplus (α_{max}) from 202.5°. The aspect (α) and slope (β) are calculated individually for each grid-cell in the DEM.

$$DAH = cos(\alpha_{max} - \alpha) * arctan(\beta) \tag{4.1}$$

4.2.2 Topographic Position Index (TPI)

The TPI describes the local concavity or convexity of the terrain. As a focal operation, the TPI considers the neighbouring pixels in a defined radius (De Reu et al., 2013). The TPI shows whether the considered raster element of the DEM is higher or lower than its neighbours within radius (R). The TPI is defined by the difference between the height of a central pixel (z_0) and the average height ($\bar{z}$) of the predefined neighbourhood (Wilson and Gallant, 2000):

$$TPI = z_0 - \bar{z} \tag{4.2}$$

$$\bar{z} = \frac{1}{n_R} \sum_{i \in Z_i}^{n} \tag{4.3}$$

If the considered pixel elevation is larger than the averaged neighbours, the TPI is positive. Positive TPI values represents ridges or peaks. On the other hand negative TPI values represent locations that are lower than their surroundings, like valleys or gullys (Weiss, 2001). The TPI shows if the pixel lies on a concave or convex surface in the predefined neighborhood. This implements in snow modeling the eolian transport of snow amounts.

The choice of the appropriate radius for TPI calculation depends on the final use and spatial resolution. Therefore, I designed a sensitivity analysis to evaluate the model performance of different TPI radii. Figure 4.3 shows the effect of different radii on the TPI. The change in the integrated neighborhood affects the range of TPI values. The histograms in Figure 4.3 show that larger radii result in higher TPI values (De Reu et al., 2013; Weiss, 2001).
Due to the different spatial resolutions depending on the model setup, the radius has to be adjusted. It is not possible to use a smaller radius then the pixel size. Otherwise no more neighbouring areas will be included in the calculations. The appropriate radius of the TPI is searched by modeling known snow distributions in different spatial resolutions. For this purpose, all model variables are included in the snow depth model and the TPI is tested with varying radii. The Feature Importance (FI) (Chapter 4.4.1) shows at which radius the snow depth model uses the TPI most as a decision maker. Accordingly, the optimal TPI radius is defined for each spatial resolution used.

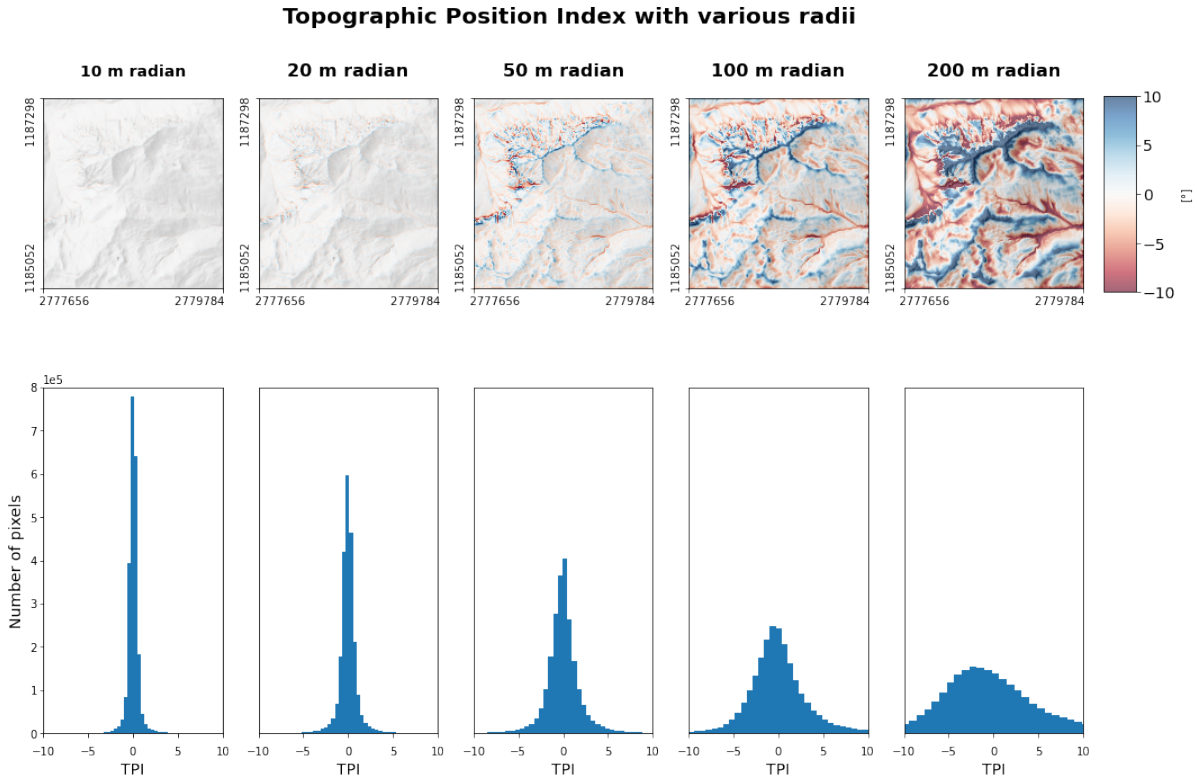

FIGURE 4.3: Topographic position index in the Latschüelfurgga region with different radii (first row). For each topographic position index map (first row), a histogram (second row) shows the difference in data distribution. By increasing the radius, more neighborhood cells are integrated into the topographic position index.

In the TPI calculations the neighborhood pixels are weighted depending on their distance. Nearby pixels influence the TPI value more than pixels with greater distances to the examination pixel. I test spatial weighting, gaussian weighting, exponential weighting and inverse weighting and decide with the FI which weighting works best for the snow modeling. The FI does not show significantly more intensive use of the TPI depending on a specific weighting. The inverse weighting with the power of two is used as the default setting in all model runs.

4.3 Data correlation analysis

To better understand the effect of acquisition timing on snow depth maps, the used snow depth maps are examined for similar spatial patterns. The correlation of the interpolated and area-wide measured snow depth is evaluated to detect possible deviations. The correlation between different model variables shows to what extent the individual variables differ to avoid too similar variables.

4.3.1 Snow depth maps analysis

In comparison to absolute HS maps, the normalized HS maps have the advantage of being independent of the absolute amount of snow. These normalized maps enable a direct comparisons of the relative snow depth distributions at different stages throughout the snow season. Comparing the normalized HS maps pixel by pixel, statistical similarity measures as the R^2 and the RMSE (Chapter 4.4.4) give a value for variability in snow distribution. This data analysis further helps to understand and interpret varying model performances pending on the temporal input data consistency. It also provides a foundation to select suitable data to train the snow depth model.

The RF-model is based on the assumption that the snow depth distribution patterns remain constant over time. To verify this assumption, all HS maps are checked for spatial correlation with each other. For this purpose, each HS map is normalized individually. The normalized HS of each recording time is calculated by the ratio of the HS in contrast to the mean snow depth of the selected area and time (Bührle et al., 2022).

$$HS_{norm.} = HS_n / mean(HS) \tag{4.4}$$

4.3.2 Correlation between interpolated snow depth from stations and area-wide measured snow depth

Interpolated HS data of the measuring stations is the only time-bound variable which is implemented in the snow depth model. It contains information about the absolute snow amounts in the study region. The snow depth interpolation is a rough HS map. The mean snow depths of the interpolated HS should correspond as closely as possible to the mean HS of the area-wide measured snow depths at the same time. By subtracting the mean interpolated HS from the mean area-wide measured snow depth, the time-related deviations become directly visible. In order to achieve an identical comparison of the mean HS of the interpolated station data and the area-wide measured HS maps, only those pixels are added to the average calculation for the interpolated HS maps which also have a measurement in the area-wide measured HS map. This direct snow comparison also serves to explain possible difficulties in modeling.

4.3.3 Random Forest-variable correlation analysis

The RF-model is based on combinations of different variables. The better a variable directly correlates to the snow distribution, the more the model uses this specific variable. The correlation analysis of the variables helps to understand the variable importance (Feature Importance FI) in the model. In contrast to the model-bound FI, the correlation analysis shows a value-independent relationship of the individual variables. Multiple strictly correlating variables can be combined or one of the similar variables can be omitted, for more efficient model building. The variables are normalized to compare data with different units. The normalization scales all variables depending on their minima and maxima between zero and one. This coefficient from Asuero et al., 2006 indicates the strength of the relationship between variables. The correlation coefficient can take values from -1 to 1 and is calculated as follows:

$$r_{xy} = \frac{\sum(x_i - \bar{x})(y_i - \bar{y})}{\sqrt{\sum(x_i - \bar{x})^2 \sum(y_i - \bar{y})^2}} \tag{4.5}$$

$\boldsymbol{r_{xy}}$ is the correlation coefficient of the linear relationship between the variables x and y. The values of the variables are called $\boldsymbol{x_i}$ and $\boldsymbol{y_i}$. The average of all values of the variables x or y is called $\bar{\boldsymbol{x}}$ or $\bar{\boldsymbol{y}}$. A close correlation between a variable and the HS map simplifies the modeling process for the snow depth model.

4.4 Random Forest regression

Random Forest (RF) is a commonly used Machine Learning (ML) algorithm for classification and regression problems. The principle of randomly generating decision trees was first introduced by Breiman, 2001. In this thesis, I use a RF-regressor from Pedregosa et al., 2011 (Scikit-learn) to model specific snow depth. Scikit-learn is a free ML-software library for the Python programming language. The RF-algorithm for classification consists of a collection of decision trees. These decision trees were generated from the training data-set using the bootstraping method. In this process, a random selection of the test data is used to define the decision nodes and snow depth in the leaves. The structure of each tree are defined by the hyper-parameters. After generating a large number of tree-structured classifiers, each tree gives the expected snow depth. By having more decision trees, the model is generalized. The model outputs the arithmetic mean of the predictions from all decision trees. Figure 4.4 shows the general flow of training and testing with the RF-regressor. The RF-model runs well on large data-sets and allows the importance of each predictor to be output in the learning procedure (Liaw, Wiener, et al., 2002). Due to the large amount of data, over-fitting is minimised (Segal, 2004). The random structure of the training data makes the algorithm sensitive to observations in the training set. A large amount of training data can stabilize the model's decisions (Segal, 2004). The principle of RF allows efficient model building with large amounts of data.

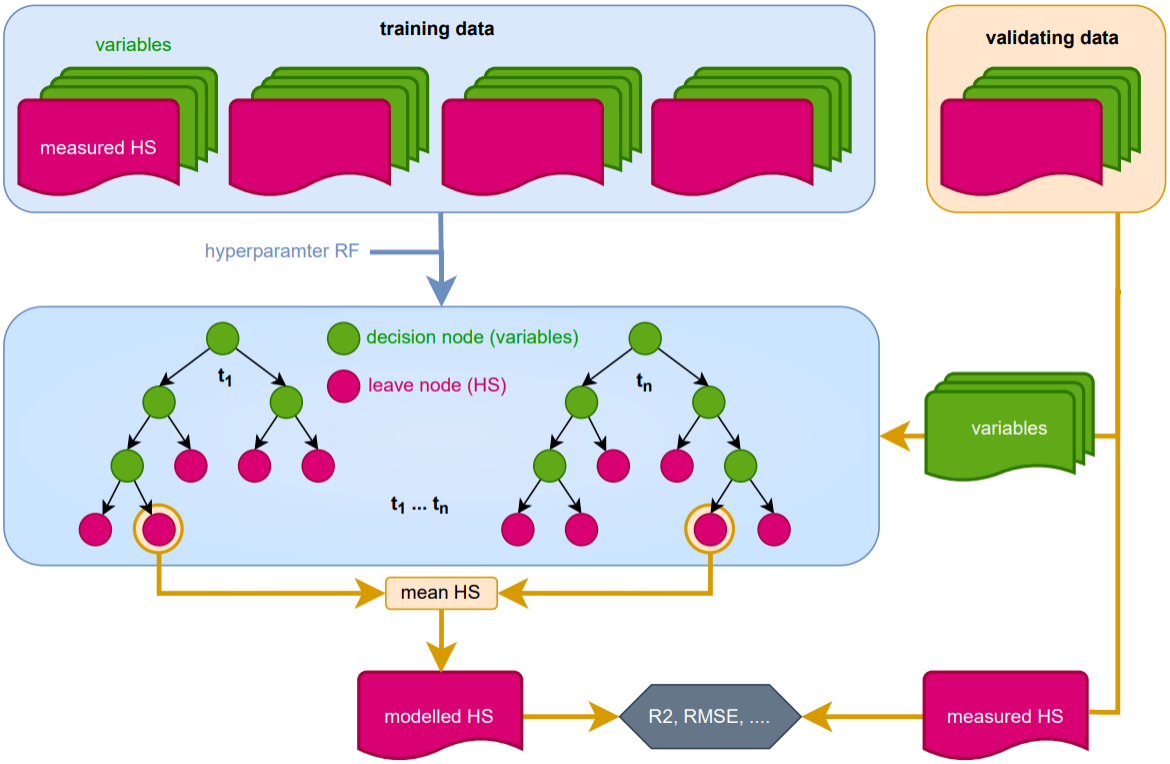

FIGURE 4.4: The flowchart shows the training and validating of the Random Forest-model. The blue colored boxes represent in training and the orange colored boxes show the application and validation of the model. Magenta symbols indicate the snow depths. Green symbols represent model variables. The model output are the modeled snow depths and statistical values (gray box) which show the model precision.

4.4.1 Feature selection

The Feature Importance (FI) defines the variable significance in the RF-model. FI is based on the Gini importance (Biau and Scornet, 2016; Strobl et al., 2007; Louppe et al., 2013). For the FI the number of separations in the decision trees based on the respective variable are counted. It is defined as the proportion of decisions in the nodes of the considered variable to all nodes. Regarding to the example tree of Figure 4.5, the FI is divided as follows: the interpolated snow depths make up 43 % (3 nodes), the SCD has a decision share of 29 % (2 nodes) and the slope and the TPI 14 % (1 node). The FI of all variables should always be 100 %. Since the RF is based on many independent decision trees, the FI of all decision trees is considered together. The FI depends only on the training data. During the model training the trees where constructed. The RF-model leaves the user nearly no information about its inner workings. Therefore, the FI brings a insight into the interior variable use of the RF-model.

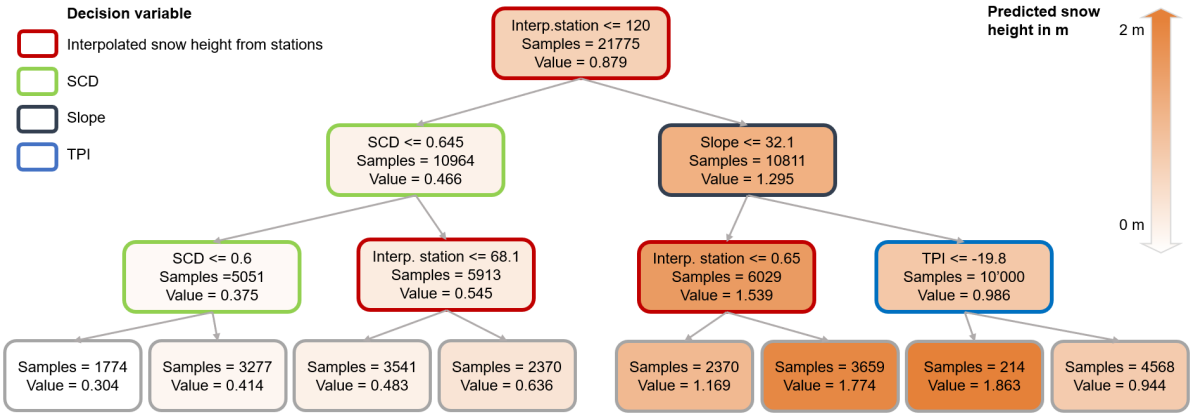

FIGURE 4.5: Example of one decision tree from the Random Forest-model. This decision tree shows a maximum depth of 3 with three levels of decisions until the tree ends in 8 leaves (last row). Each leaf contains the number of samples, meaning how often this node is used for decision, and the predicted model output, in this case the predicted snow height. This decision tree shows 4 types of decision, marked with the colored edging. The node has a red edging if the decision base on interpolated snow height form stations, green if the decision base on snow cover duration, dark blue if the decision base on the slope and bright blue if the decision base on the Topographic Position Index.

4.4.2 Hyper-parameter tuning

Hyper-parameters predefines the structure of the decision trees and the number of trees in a RF-model. The RF-principle can only be influenced in a limited extent. In addition to the training variables, the user can define the number of decision trees and their rough structure. Maximizing the number of decision trees increases the computation time, but minimizes the variability between the individual model runs (Luo et al., 2022). To compare the results independent of the model settings, I use the following hyper-parameter settings for each experimental setup:

- Absolute number of single decision trees: 300 trees
- Maximum depth of the tree: 10 nodes
- Minimum number of samples to separate a node: 2 samples
- Minimum number of samples in a leaf (a separation is only done if this minimum number of samples is included in the resulting leaves): 1 sample
- Maximum number of features that will be checked when splitting the tree: 6 variables

These hyper-parameters were defined by an automatized process of many model runs. In each model run, different hyper-parameters were tested and the model precision was checked using statistical parameters. The hyperparameters were tested at predefined intervals. The different combinations of hyper-parameter values are then checked for the suitability of the decision tree. This process is repeated several times until the RF hyper-parameters settings for the testing data set no more improve. Statistical values are used in modeling to represent the model precision and therefore select the best hyper-parameters. The number of features used must be adjusted manually. By optimizing the hyperparameters based on the statistical values, the diversity of snow modeling can be lost. The model tends to use few variables and to model a homogeneous snow depth close to the mean. In this way, the statistical quantities of the

resulting snow depth maps improve, but deviate more from the measured validation maps. Accordingly, the number of variables to be used in the hyperparameter optimization process was predefined to 6 variables.

4.4.3 Training procedure

A large and diverse data-set for training the RF-model is crucial for accurate snow depth modeling. The spatial dimension of the data structure is removed for training and validating the RF-model. Pixel locations that feature a data gap in one of the variables must be completely excluded from the training process. The flowchart in Figure 4.4 shows that the available data are differentiated into training and validating data. The k-fold cross-validation (k-fold CV) (Stone, 1974) is used to divide training and validation data. The k-fold CV corresponds to the number of available snow maps at different recording times. In k-fold CV, one snow depth map is used as validation data and all other available maps of the considered region are included in the model training. In a next run, a new validation time is used and all other available snow depth maps are used to train the model. With the k-fold CV method all time points are used for the validation and the model training. Depending on the modeling question, the data set of the Davos region from one point in time was used for validation and the others for training the model. For the transferability analysis all available snow depth maps of the Davos region were used for training and the respective extrapolation region for validation of the RF-model. The snow depth maps (Flowchart 4.4 in magenta) are separated from the other variables (Flowchart 4.4 in green). The snow depth maps are the leaves to be achieved in the RF decision tree. The following variables are used for the decision nodes:

- Elevation
- Slope
- Aspect
- Diurnal Anisotropic Heat index (DAH)
- Topographic Position Index (TPI) (radius depends on the spatial resolution)
- Snow Cover Duration (SCD)
- Interpolated snow depth from measurement station

The leaves are based on the values of the HS-maps. The training set does not include the scan-based snow depth information at the time of modeling.

4.4.4 Evaluation metrics

To verify the settings and precision of the RF-model, I use statistical quantities from the measured and modeled snow depth distribution. Frequently used statistical values in snow models are: coefficient of determination (R^2), Mean Absolute Error (MAE), Median Absolute Deviation (MAD), Root Mean Square Error (RMSE) and the Regression Line Slope (RLS) (Bührle et al., 2022; Revuelto et al., 2020; Grünewald et al., 2013; Sturm and Wagner, 2010; Hu et al., 2021; Daudt et al., 2022). The determination coefficient R^2 represents the ratio between the dependent and the independent variable. The R^2 indicates how much scattering of the data can be explained by the RF-model. The better the modeled values fits on the predicted line, the closer is the R^2-value to one. R^2 is the deviation of the residual sums of squares (SS_{res}) by the total sum of squares (SS_{tot}) (Miles, 2005). The SS_{res} is the residual sum of squares (blue line in Figure 4.6). The SS_{tot} explains the proportional to the variance of the data (yellow line in Figure 4.6).

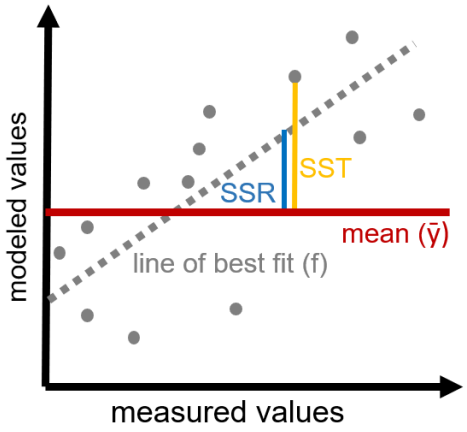

$$SS_{res} = \sum_i (y_i - f_i)^2 \tag{4.6}$$

$$SS_{tot} = \sum (y - \bar{y})^2 \tag{4.7}$$

$$R^2 = 1 - \frac{SS_{res}}{SS_{tot}} \tag{4.8}$$

FIGURE 4.6: Scatter plot showing predicted versus measured data. The SS_{tot} represent the yellow squared residuals with respect to the average value. The blue square represents the residual to the linear regression. The better the linear regressor (dotted line) fits the data in comparison to the simple average (red line), the closer the value R^2 is to one.

The Mean Absolute Error (MAE) is a scale-dependent metric that measures the average absolute error between a set of predictions and their ground-truth labels. The unit of the statistic coefficient is similar to the modeled unit of the snow height. It includes estimates based on the calculation, where y_i is the measured values at position in, $f_i^{(RF)}$ is the obtained value at position i from the RF-model with n elements.

$$MAE = \frac{1}{n}\sum_i^n (y_i - f_i^{(RF)}) = mean(y_i - f_i^{(RF)}) \tag{4.9}$$

Similar to MAE, the Median Absolute Deviation (MAD) is a robust statistical metric of the model-error which ignores highly erroneous predictions by taking the median instead of the mean. For the MAD, the obtained value at a specific position is subtracted by the measured value at the same position. Than the median of this difference between all possible position is calculated:

$$MAD = median(y_i - f_i^{(RF)}) \tag{4.10}$$

The Root Mean Square Error (RMSE) is the standard deviation of the residuals. These residuals represents the distance between the data points and the regression line (Miles, 2005). The RMSE shows how distributed the predicted versus measured data form an optimal regression line are.

$$RMSE = \sqrt{\frac{1}{n}\sum_{i}^{n}(y_i - f_i^{(RF)})^2} = \sqrt{mean(y_i - f_i^{(RF)})^2} \tag{4.11}$$

The qualitative analysis of model precision helps to compare the different model runs. To see a tendency towards snow over- or under-estimation, I use the Regression Line Slope (RLS). Figure 4.7 shows each pixel of the snow maps as a point depending on the measured and modeled snow amount. The black one-to-one line represents a perfect model, where the model predicts for each grid point exactly the measured snow depths from test data. The red regression line indicates the best fit trough the scatter points with the minimum distance between the scatter points and the regression line. The regression line is fixed at the origin. The deviation of the RLS to one, shows the tendency towards over- or underestimation of snow amounts by using the model. Information about the dispersion of the point cloud are contained in the other error measures like the RMSE or the R^2.

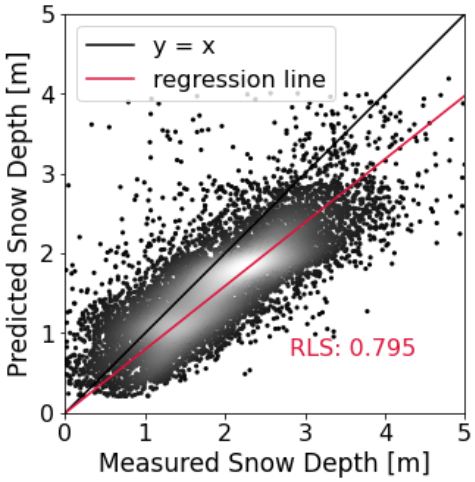

FIGURE 4.7: Scatter plot showing predicted versus measured height of snowpack (HS). The black line (one-to-one line) represents a perfect model (perfect prediction) with a slope equals one. The red line represents the real trend line, fitted through the data points. A slope lower than one indicates an underestimation of the height of the modeled variable, in my case the height of snowpack.

In addition to the statistical quantities, I also compare the modeled snow depths with the snow depth map from the aerial photographs. In this way, terrain-based difficulties can be noticed and processed. The visual analysis of the model results focuses mainly on the distribution and spatial patterns of the snow amounts. This is especially important for the end use of the snow depth maps namely avalanche forecasting. Not only the absolute modeled snow-mass in a large area is of interest, but especially the snow depth distribution.

5 Results

5.1 Data analysis

5.1.1 Measured snow depth analysis

The RF-model bases on similar snow distribution at different times. At the beginning of winter the snow distribution is more homogeneous compared then at the second half of the snow season. In all five snow depth surveys of the Latschüelfurgga (Figure 5.1) rough spatial patterns of snow accumulation are evident, such as in the trough in the northeast of Latschüelfurgga (blue in all five snow depth maps in Figure 5.1).

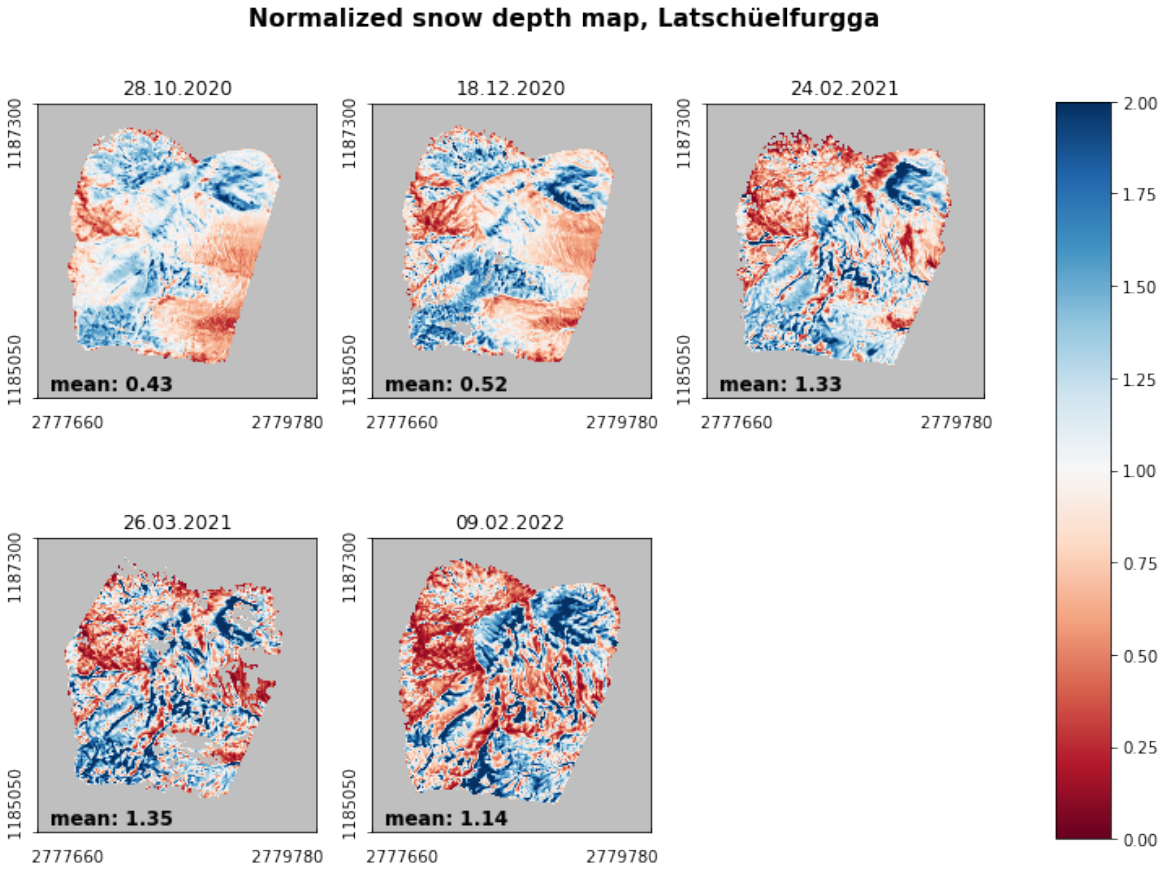

FIGURE 5.1: The five snow depth maps are normalized with the mean measured snow depth of the respective recording time. If the snow depth of the pixel corresponds to the mean, the normalization becomes one (white). Areas with less snow than the mean are colored red whereas blue areas have more snow than the mean. The less intense colors in October and December represent a more homogeneous snow distribution at the beginning of the snow season.

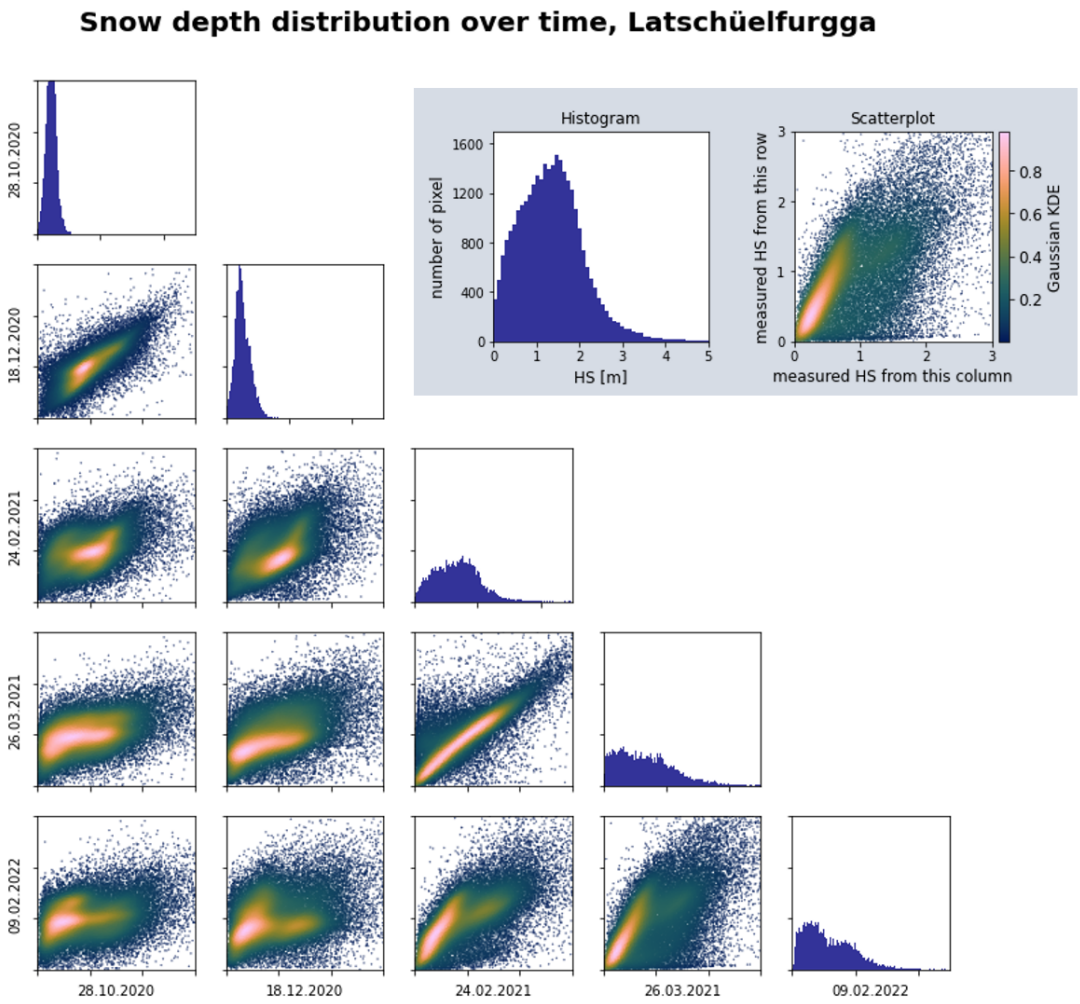

FIGURE 5.2: The scatter plots show the pixel-by-pixel correlation analysis of the five snow depth maps from the Latschüelfurgga. The point cloud density is colored by the kernel density estimation. The histograms represent the number of pixels over the measured snow depth map. The Kernel Density Estimation (KDE) is color-coded. The histograms represent the number of pixels per modeled snow depth.

The pixel-wise based analysis (Figure 5.2) of the five snow depth maps without normalization (Figure A.1) support qualitatively (Table 5.1) the observations of Figure 5.1. The two measurements taken at the beginning of the snow season in October and December contain mostly snow depths below 2 m. The histograms in Figure 5.2 show more even distribution of the number of pixels over all snow depths in the second have of the snow season (24.02.2021, 26.03.2021 and 09.02.2022). The R^2 and RMSE value in Table 5.1 represents, a similar snow depth distribution on the 28.10.2020 and the 18.12.2020. The two temporally close snow depth maps from 24.02.2021 and 26.03.2021 correlate best with each other. The point cloud is partly divided into two areas as shown in Figure 5.2 in the scatter plots of 09.02.2022. In certain areas the measured snow amounts correspond well with snow depths from another point of time. The splitting of the point cloud also shows regions in which there are time-related differences. The statistical values in Table 5.1 supports the observation from the normalized HS map in Figure 5.1 by showing a difference of the snow distribution during the snow season.

TABLE 5.1: R^2 and RMSE oft the correlation analysis between the measured snow depth maps in the Latschüelfurgga region. The R^2 values in the lower part of the table indicates with lower R^2 (colored in darker blue) different snow depth distribution between the observed snow depth maps. Bigger R^2 values (colored in withe) describes more equal snow distributions of the observed snow depth maps. The RMSE values are located at the top right of the table and are colored green. Smaller (brighter colored) RMSE values indicate more similar distribution of snow amounts at the two considered time points. A close correlation exists between 28.10.2020 and 18.12.2020.

	28.10.2020	**18.12.2020**	**24.02.2021**	**26.03.2021**	**09.02.2022**
28.10.2020		0.07	0.24	0.31	0.36
18.12.2020	0.61		0.23	0.30	0.40
24.02.2021	0.19	0.25		0.17	0.22
26.03.2021	0.26	0.30	0.59		0.33
09.02.2022	0.11	0.09	0.44	0.35	

The same snow distribution analysis based on the snow depth maps was also performed with all data used for Schürlialp as well as for the Davos region (corresponding Figures in Appendix A). The normalized snow depth maps (Figure A.3) represents homogeneous snow cover on the valley floor in the center of the study area. Both sides of the slope are interspersed with snow-filled gullies and blown edges. The R^2 and RMSE of the Davos region (Table A.2) indicates that the snow distribution of January 2016 differs from other snow maps. Also the shape of the point cloud (Figure A.7) reflects this difference.

The spatial comparison of the individual recordings shows that the snow distribution mostly adopt similar patterns. Therefore, the RF-model can model the snow distribution time independently.

5.1.2 Mean comparison of measured versus interpolated HS

The interpolated snow depths of the measuring stations are the only time-bound data which is included in the RF-model. They represent the general snow situation at the observed time in the RF-model. There is no clear tendency of a general over- or underestimation of the snow depth by the interpolated station data (Figure 5.3). The mean snow depths of the interpolation tend to agree better with the mean snow depth from HS maps at the beginning of the snow season. From February on, the dispersion between the two mean snow depths increases. There are no clear tendencies between the analyzed regions. The five considered time points of Schürlialp show large differences. On average, the mean value of the interpolated snow depths is 26 cm next to the mean measured snow depths. The interpolated station data underestimate the measured snow depths by 6 cm. This comparison of mean values shows how representative the interpolated snow depths are for the absolute snow amounts. The analysis can infer possible deviations of the modeled snow depths.

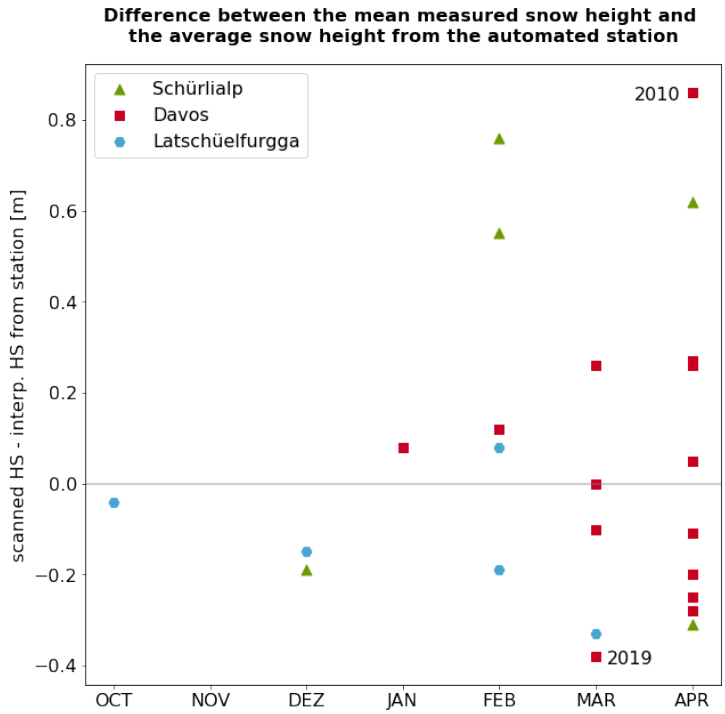

FIGURE 5.3: The difference between the mean area-wide measured snow depth and the mean interpolated snow depth of the measuring stations defines the position along the y-axis. The x-axis distinguishes the point in time considered in the snow season. The colors and shapes separate the large Davos region (red squares) from the smaller Schürlialp (green triangles) and Latschüelfurgga (blue circles) regions which are located within the large Davos region. The deviation of the compared mean values ranges often between -40 cm and 40 cm.

5.1.3 Model-variable correlation

The model-variables correlates slightly with each other. The strongest positive correlations are between the elevation and the SCD as well as between the two TPI with different radii (Figure 5.4). The two snow depth maps, interpolated snow depths from the stations as well as the area-wide measured snow depths, are compared in chapter 5.1.2. A close correlation between the snow depth map and an other variable does not appear. The RF-model combines these variables correlating with snow depth in the decision trees to generate a modeled snow depth map.

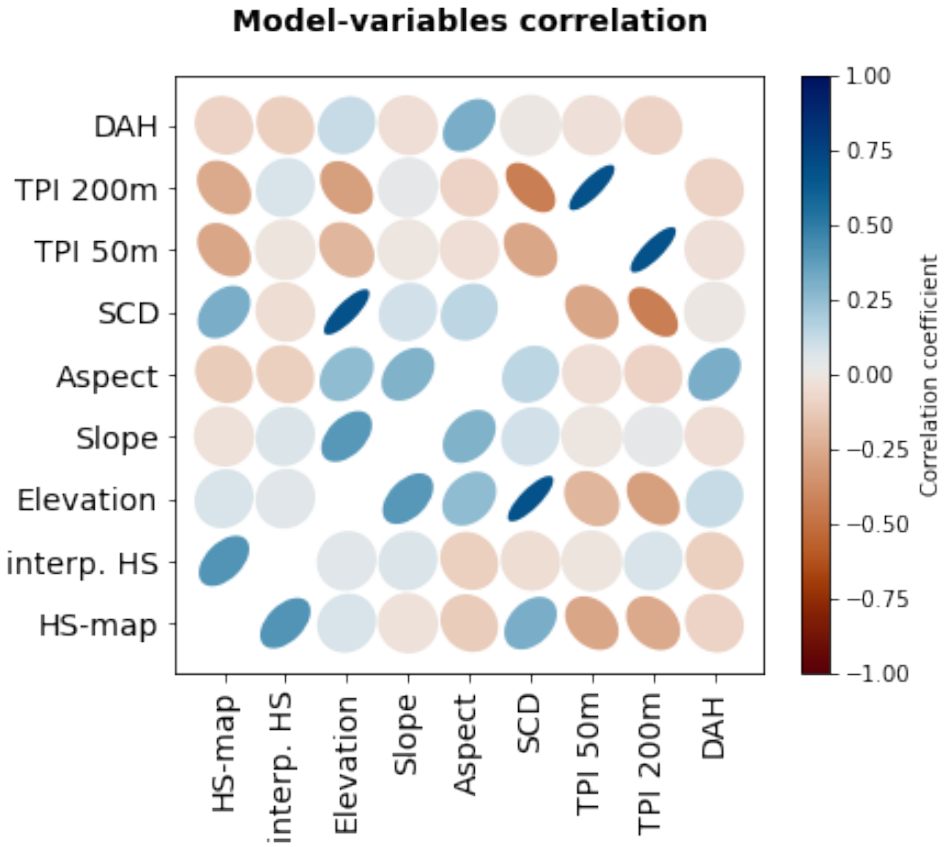

FIGURE 5.4: All model variables are tested individually against each other for their covariance. More intense color and a more oval shape represent a stronger correlation. Negative correlation are colored in ocher, positive correlation in blue. This correlation analysis includes model variables of the Davos region at different times with a spatial resolution of 10 m.

5.2 Variable importance

The Feature Importance (FI) is used to understand the significance of the variables in the RF-model. Based on the FI, I select a suitable radius to calculate the Topographic Position Index (TPI) at different spatial resolution. In addition, changes in FI at different spatial resolutions are considered. In addition, FI was examined in different study regions.

5.2.1 Topographic Position Index (TPI) radius with changed spatial resolution

The TPI represents the curvature of a pixel by observing its neighborhood. By implementing a predefined radius the included neighborhood area varies. The FI helps to find the most representative radius for the snow depth of a certain region. The choice of the radius depends on the spatial resolution of the grid. Figure 5.5 indicates the tendency towards larger radii which include more neighboring pixels.

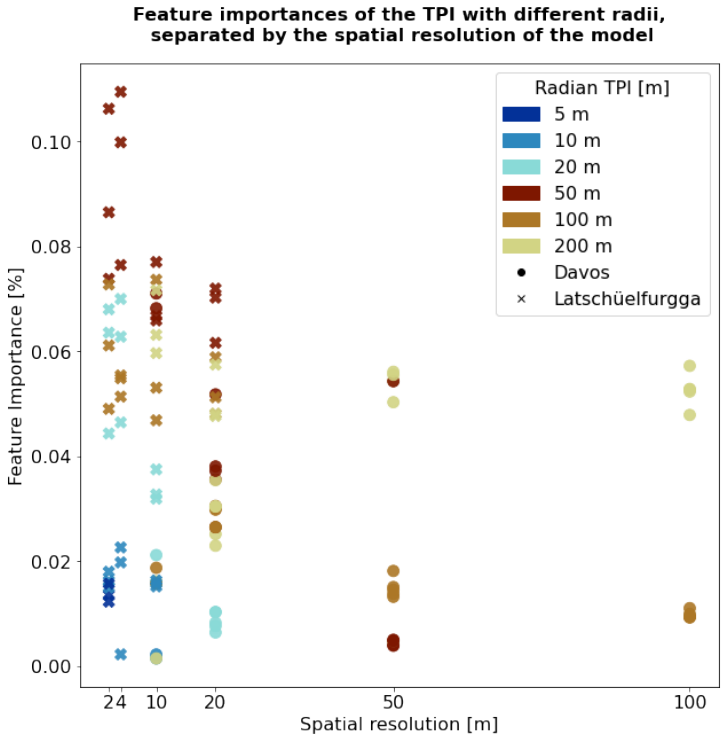

FIGURE 5.5: The feature importance from the topographic position index of Davos (points) and Latschüelfurgga (crosses) is plotted against the spatial resolution. The radius used for this purpose defines the included neighborhood area and is distinguished by the color scale. Larger radii tend to achieve a greater feature importance.

The results of these TPI analyses with different radii at different resolutions are used to define the basic settings of the RF-model. For a spatial resolution of 20 m or smaller, the TPI result of 50 m radius is applied. The resolutions with pixel edges longer than 20 m are trained in the RF-model by TPI with radius 200 m.

5.2.2 Differences in variable importance depending on the spatial resolution

The spatial resolution influences the composition of the decision trees in the RF-model. Figure 5.6 shows the interpolated snow depths from the measurement station data (interp. HS) and SCD have a higher FI than the topographic variables (elevation, slope, aspect, TPI and DAH). The percentage of decisions based on topographic variables is only 23%. The other 77% are distributed to the interpolated snow depths (34%) and to the SCD (43%).

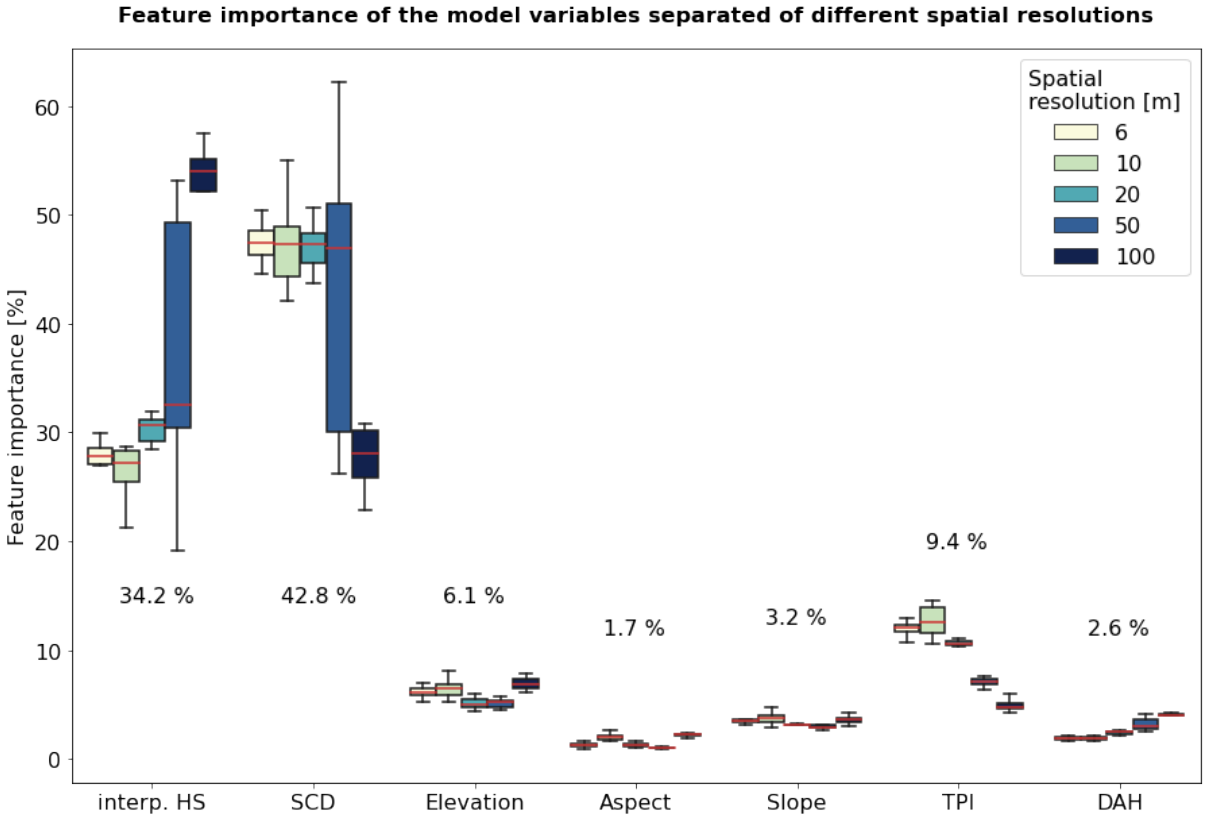

FIGURE 5.6: The box plots shows the Feature Importance (FI) against the different variables. The Figure includes only the Davos region. Out of the 14 exposures, one was modeled and the other 13 are used to train the model (k-fold cross validation). The boxes are colored according to the spatial resolution of the grid.

In addition to the general distribution of FI in the RF-model, Figure 5.6 shows the differentiation of FI at changing spatial resolution. The FI of the two variables with the highest FI (interpolated HS and SCD) differed most depending on spatial resolution. The FI of the interpolated HS increases strongly with coarser spatial resolution especially at a pixel size of 50 m and 100 m. In contrast to the interpolated HS, the FI of the SCD decreases with coarser spatial resolution. A similar trend can be observed for the TPI. The DAH shows a slight increase of the FI with increasing pixel size. The FI of elevation, slope and aspect does not change with variation of spatial resolution.

The scatter of the FI for the different model training is overall very narrow. The boxes in Figure 5.6 are mostly small and the outlier markings are close to the edge of the box. In general, the lower the FI, the smaller the deviation. The FI of the interpolated snow data as well as the SCD at a spatial resolution of 50 m show larger deviations. The 50 m edge length of the pixel seems to be a connection in the change of the FI between more detailed modeling and coarser raster cells. This shows that at a spatial resolution of 50 m, the decision trees in the RF-model differ greatly.

5.2.3 Influence of the study area on the parameters importance

To compare the FI between different study regions, the RF-model is trained with all available scans (Table 3.1) of the respective study regions. The training of the RF-model influences the FI. The bar chart (Figure 5.7) shows the proportions of the decisions of the respective variables in different sub-regions.

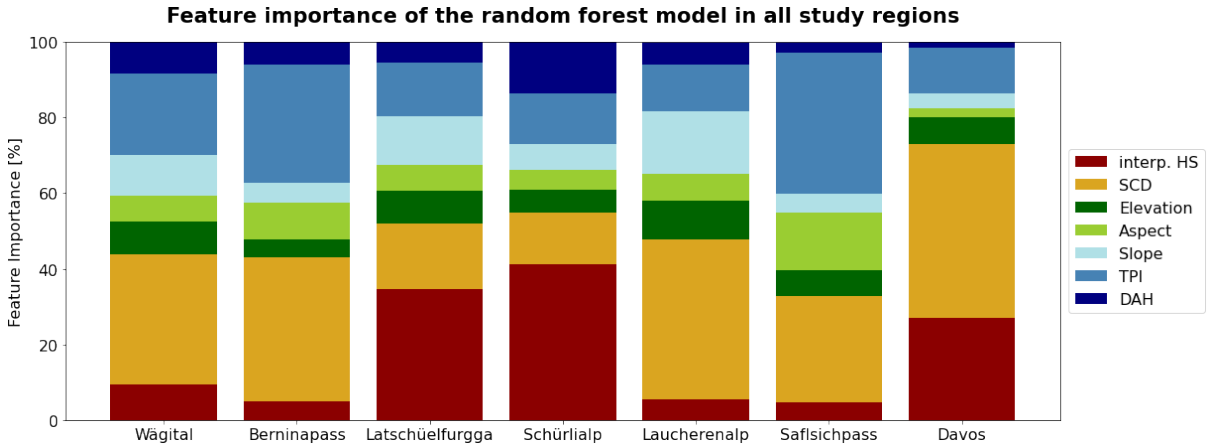

FIGURE 5.7: The coloring of the bars divides the Feature Importance into the different variables whereas the individual bars represent the seven different regions. The feature importance values are an average of model runs depending on the timing of the available height of snow depth maps. The spatial resolution of all model runs is 10 m edge length.

The Saflischpass, Berninapass, Laucherenalp and Wägital study areas are only trained with one or two reference snow depth map. Davos, Latschüelfurgga and Schürlialp contain at least five reference scans from different years. Depending on the number of reference snow depth maps per region (Table 3.1), the number of training varies. Figure 5.7 shows the mean FI of all training.

TABLE 5.2: Average feature importance of all study regions.

Model variable	Average FI [%]
iterp. HS	18.2
SCD	31.4
Elevation	7.4
Aspect	7.7
Slope	8.7
TPI	20.3
DAH	6.3

Table 5.2 serves as general reference for the average distribution of the FI at all study areas. Table 5.2 shows two groups of variables. First, the interpolated HS, SCD and the TPI each account for about 20% of the decision. Second, topographic variables of elevation, aspect, slope and DAH contain about 7% importance.

5.3 Model accuracy at different spatial resolutions

The R^2 value increases with coarser spatial resolution (Figure 5.8). In contrast, the Root Mean Square Error (RMSE), Mean Absolute Error (MAE) and Median Absolute Deviation (MAD) of the 14 modeled time points decreases with increasing resolution (Figure 5.8 and Table B.1). The R^2, RMSE, MAE and MAD values indicate, that the model accuracy decreases with increasing precision in spatial resolution. Looking separately at the R^2 and RMSE values of each modeled point in time (Figure 5.9), we observe there are no temporal differences over the FI depending on the spatial resolutions (Figure 5.9). The RF-model accuracy statistically decreases with more detailed spatial resolution. The R^2 and RMSE vary greatly between the different time points. These temporal variations are often present in all spatial resolutions (Figure 5.9).

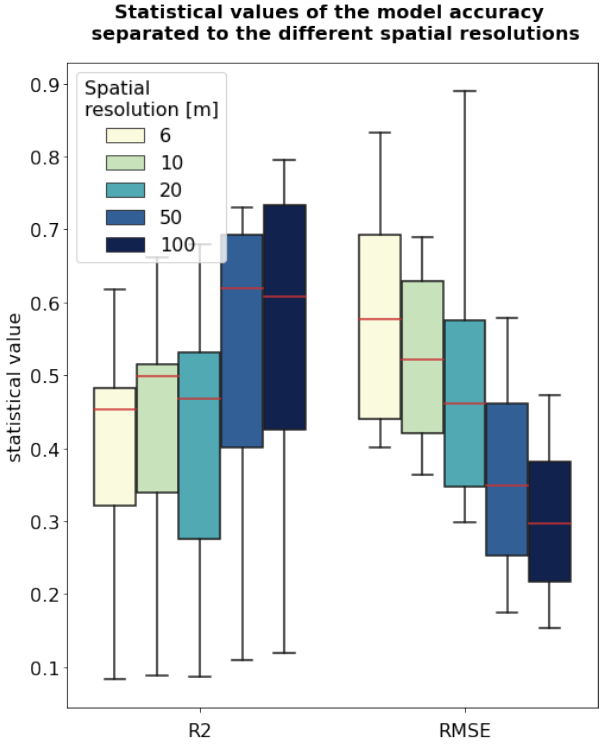

FIGURE 5.8: A box contains the R^2 (left) and RMSE (right) values of all 14 modeled time points of the Davos region. They are differently colored based on the spatial resolution. With increasing pixel size (towards darker colors), the R^2 increase and the RMSE value decrease. This indicates a better statistical model precision at coarser spatial resolution.

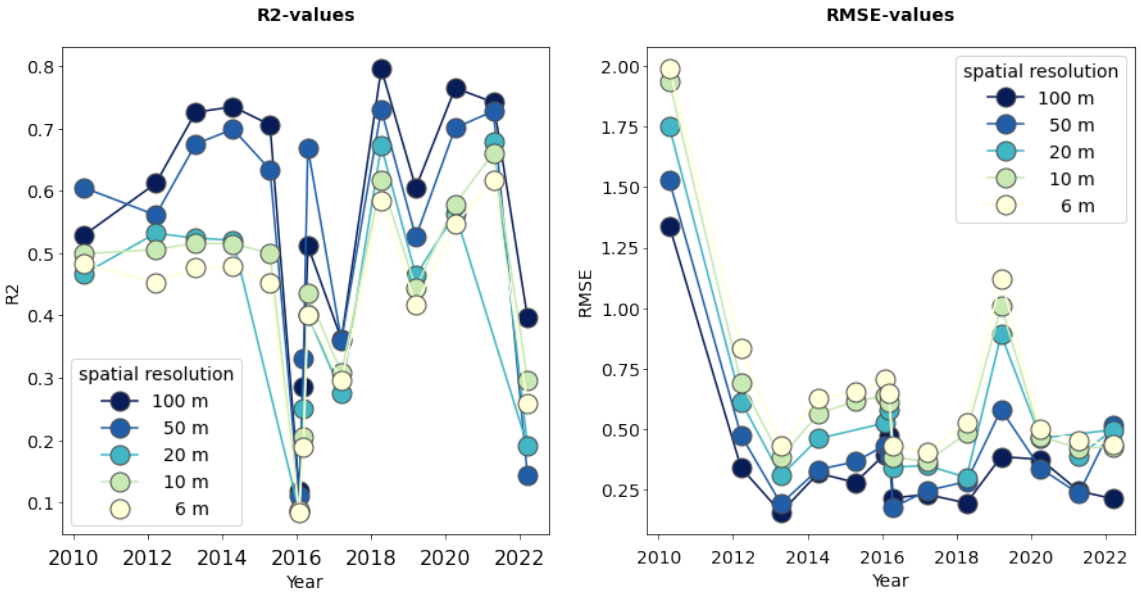

FIGURE 5.9: Evolution of R^2 and RMSE values from 2010 to 2022: the colors indicate different spatial resolutions form coarse resolution (dark blue) to detailed resolution (bright beige). The model precision changes depending on the modeled time mostly in all spatial resolutions.

Modeling at different resolutions also affects the spatial distribution of snow. Figure 5.10 shows a direct comparison of area-wide measured and modeled snow depth at different spatial resolutions. The example region in Figure 5.10 is located in the southern part of the Dischma valley in the Davos region. The less detailed variation in the modeled snow map (second column in Figure 5.10) indicates a stronger snow depth correlation with the elevation in the modeled maps the in the measured snow depth maps (first column in Figure 5.10). The RF-model has difficulties to model the small-scale structures contained in the fine-resolution data. Merging pixels to achieve coarser spatial resolution results in lower extremes in snow depths (scatter plot Figure 5.10). The maximum of the measured snow depths decreases with coarser spatial resolution. In contrast, the minimum measured snow depth increases with larger pixels. Since no points in the scatter plot of Figure 5.10 are placed in the lower region indicates that there are no snow depth modeled below 80 cm. The limited modeling of snow depths is especially noticeable at more detailed spatial resolutions such as 6 m and 10 m pixel size. In addition to limiting the low snow depths at about 80 cm, a maximum snow depth of 4.5 m is modeled at fine resolution of 6 m. The Regression Line Slope (RLS) (red line in scatter plot, Figure 5.10) becomes steeper with coarser spatial resolution. A regression line steeper than one, indicates a tendency to overestimate the snow amounts in the model. The coarser the spatial resolution, the more the amount of snow is overestimated in the RF-model.

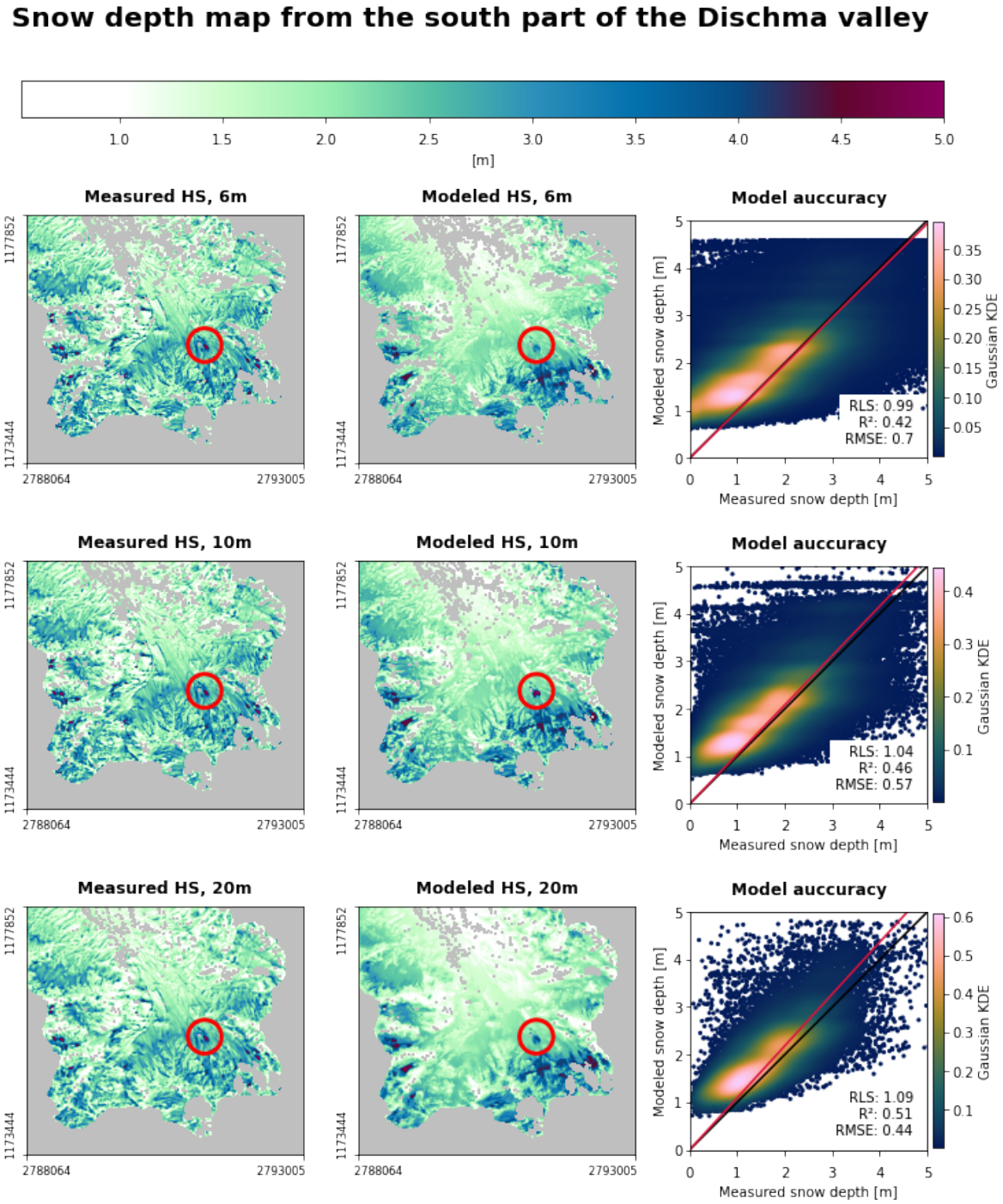
Snow depth map from the south part of the Dischma valley
1.0
1.5
2.0
2.5
3.0
3.5
4.0
4.5
5.0
[m]
Measured HS, 6m
Modeled HS, 6m
Model auccuracy
1177852
1173444
2788064
2793005
Modeled snow depth [m]
Measured snow depth [m]
Gaussian KDE
RLS: 0.99
R²: 0.42
RMSE: 0.7
Measured HS, 10m
Modeled HS, 10m
Model auccuracy
RLS: 1.04
R²: 0.46
RMSE: 0.57
Measured HS, 20m
Modeled HS, 20m
Model auccuracy
RLS: 1.09
R²: 0.51
RMSE: 0.44

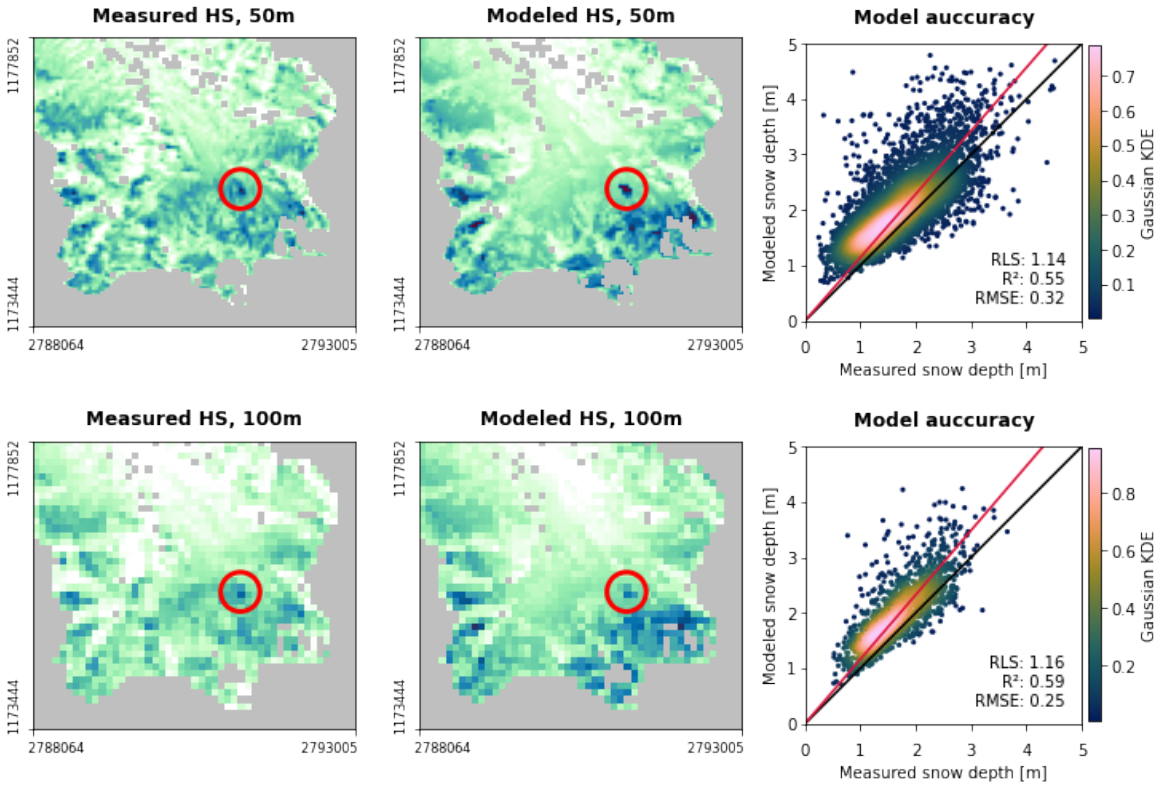

FIGURE 5.10: The measured and modeled snow depths are compared at different spatial solutions from the 06.04.2020. The represented area is a part of the Davos region located at the southern part of the Dischma valley. The scatter plot compares the modeled snow depth with the measured snow depth pixel by pixel. The position of the points in the scatter plot depend on the measured snow depth of a pixel (x-axis) and the modeled snow depth at the same pixel (y-axis). The black one-to-one line shows the modeled and measured snow depths coincide. The red regression line shows the optimal correlation of the point cloud. The Regression Line Slope (RLS), coefficient of determination (R^2) and Root Mean Square Error (RMSE) are three statistical values to describe the model accuracy. The color of the point cloud corresponds to the kernel density estimation (KDE) and shows the density of the point clouds.

5.4 Inter- and intra-annual snow depth modeling

The model accuracy of the RF-model decreases if there are seasonal differences between training and testing data. Suitable test data sets are important for good and accurate modeling. To obtain a generally trained RF-model, the model is trained with all 14 snow depth maps of the Davos region. This is done at a spatial resolution of 10 m. The large training region with 14 sampling times should result in a stable trained RF-model. The RF-model is tested at five images each from Latschüelfurgga and Schürlialp. These images are not always taken at the time of maximum snow peak (Table 3.1). The two regions Latschüelfurgga and Schürlialp are located in the Davos training region (Figure 2.1), so no spatial extrapolation is available between the training and validation area. Figure 5.11 shows the RLS compared to the measured snow depths. The steep regression lines in October and December (Figure 5.11) show that none of these snow amounts are generally too heterogeneously distributed. The regression line flattens out as the length of the snow season increases. According to the RLS, the model accuracy improves in the second half of the season.

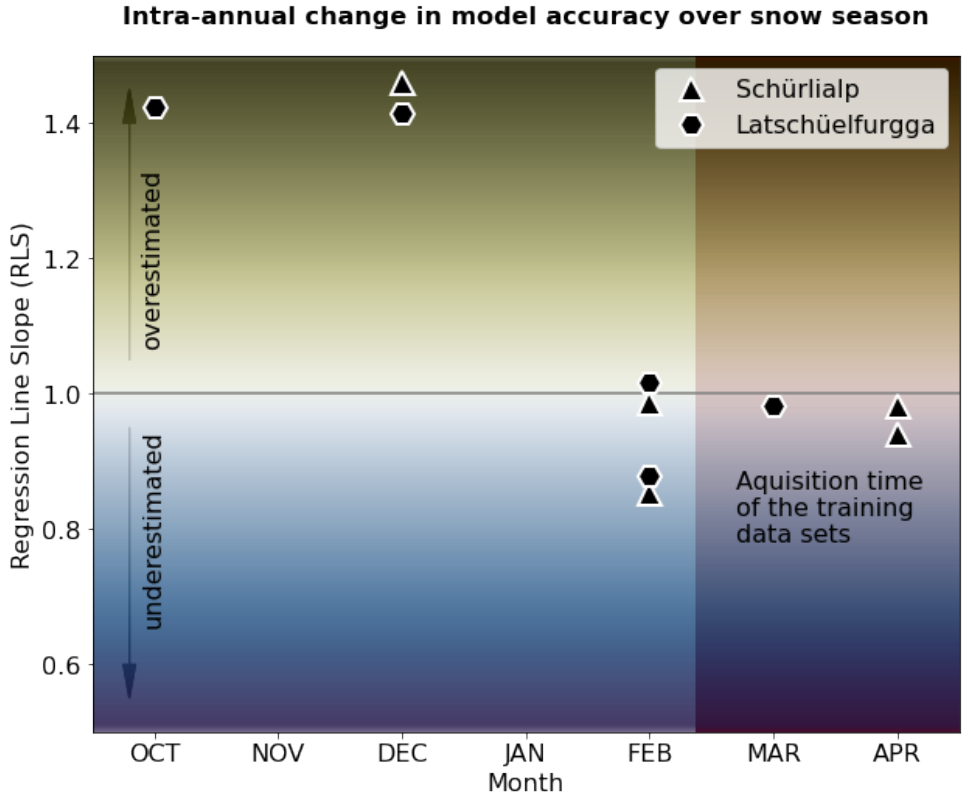

FIGURE 5.11: The position along the y-axis shows the Regression Line Slope (RLS) between modeled and measured snow depth values. The x-axis represents the monthly evolution over the snow season. The Schürlialp and Latschüelfurgga snow models are modeled with the RF-model trained in the Davos region with 10 m spatial resolution. The dark marked area in March and April shows the lapse of time from the training data. There is an overestimation of the snow amount at the beginning of the snow season. In the second half of the season, the model tends to underestimate snow depth.

In addition to the comparison of the model precision within a snow season (intra-annual), the results between the considered years are compared (inter-annual). The snow depth maps of the Davos region were always recorded at a similar time relative to the snow accumulation in the snow season. Figure 5.12 shows the RLS for all modeled snow depths in the Davos region. Most RLS are less than one. The average RLS over all is 0.87, which also indicates a generally too homogeneous distribution of the snow by the RF-model. Figure 5.12 shows the RLS in the lower (blue) part, which deviates much more from one.

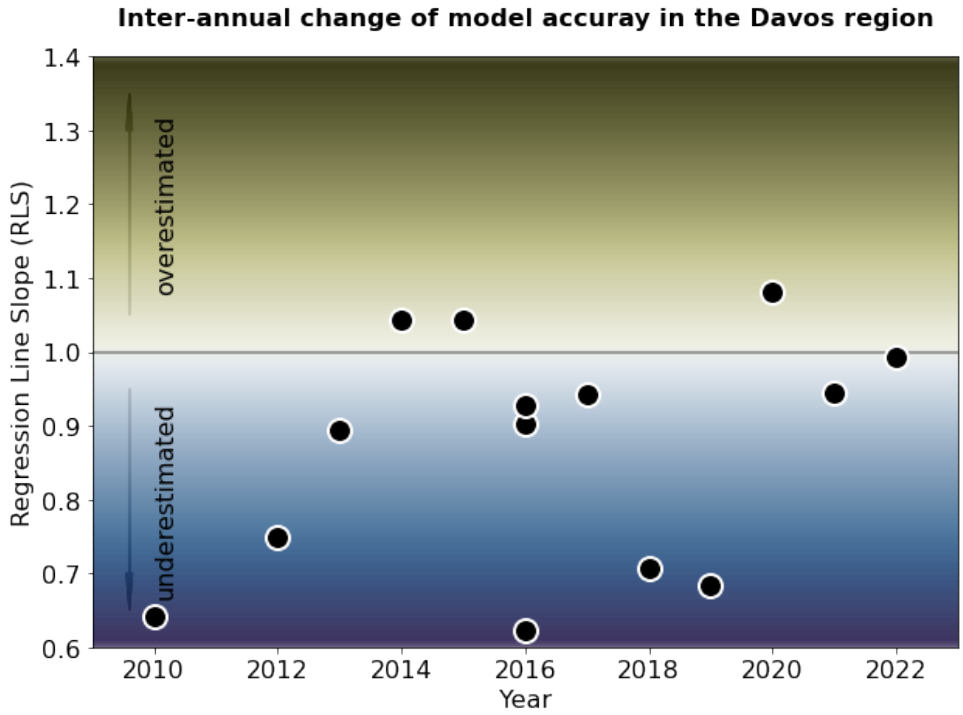

FIGURE 5.12: The evolution over 13 years of model precision based on the Regression Line Slope (RLS) shows a underestimation of the modeled snow amount. Most of the points lie below one. Therefore, the model distributes the snow too homogeneously. Each point corresponds to a model output whereas the RF-model is trained with the 13 other time points by using the k-fold cross validation.

5.5 Random Forest model transferability

The main goal is to apply the trained snow model to an arbitrary region. In the following section, the RF-model trained in the Davos region is used to predict snow depths in four different Alpine regions. Time and space differ between the modeling and training data. The statistical values in Table 5.3 depend on the study regions. The measured compared to the modeled snow depth map shows the modeling potential and difficulties. Increased snow amounts in large gullies are well modeled (Figure 5.13 a). The extremely heterogeneous distribution of snow amounts measured in April 2012 on the Berninapass (Figure 5.13 b) cannot be reproduced by the RF-model (Figure 5.13 a). The scatter plot (Figure 5.13 d) supports the mentioned (from the inter-annual analysis in Figure 5.12) too homogeneous snow distribution of the model. The increase snow depth with increasing elevation is clearly visible in Wägital (Figure C.2) and Laucherenalp (Figure C.3). The low R^2 value of the Wägital and Lauchernalp shows an imprecise model result. The higher R^2 of 0.508 in the Saflischpass region (Table 5.3) indicates different precision modeling depending on the test region. The heterogeneous measured snow distribution at Saflischpass (Figure C.1) is modeled more homogeneous (Figure C.1). This too homogeneous distribution of snow masses by the RF-model is already known from the Berninapass as well as the inter-annual comparison (Chapter 5.4). The three statistical quantities in Table 5.3 indicate how differently precise the snow depth modeling is in the four considered regions. Also the comparison region Davos-North does not achieve outstandingly better results. This tells us how important it is to use a representative training data set.

TABLE 5.3: Statistical values (R^2, RMSE, Regression Line Slope (RLS)) of the transfer regions by using a RF-model, trained in the Davos region with 14 snow depth maps of a spatial resolution of 10 m. This model is applied to the four Alpine test regions Wägital, Saflischpass, Laucherenalp and Berninapass. As a reference, the Davos region itself is divided into a southern training zone and a northern testing region (Davos North). Due to the different availability of snow surveys, the statistical values are the average of different initial models: Davos North 14, Wägital two and Laucherenalp, Saflischpass and Berninapass one each.

	R^2	RMSE	RLS
Davos North	0.396	0.559	0.878
Wägital	0.296	1.619	0.432
Saflischpass	0.508	1.584	0.657
Laucherenalp	0.281	1.165	1.082
Berninapass	0.42	0.4	0.825

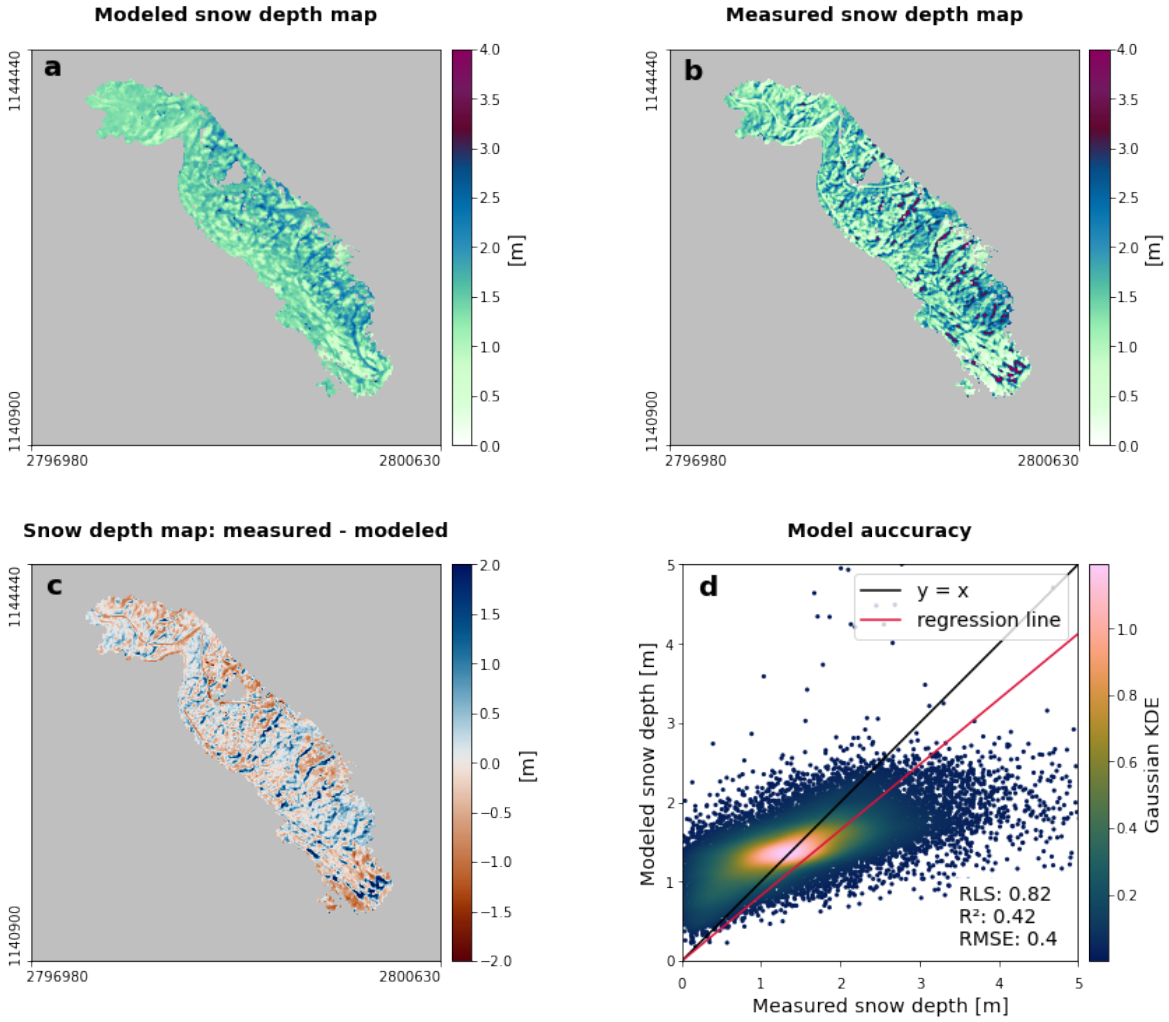

FIGURE 5.13: For all plots, the model was trained exclusively with data from the Davos region. (a) modeled snow depth distribution of the Bernina region (b) reference snow depth map used for model precision (c) difference between the measured snow depth an the modeled snow depth (d) snow depths model precision. The position of the points (d) depend on the measured snow depth of a pixel (x-axis) and the modeled snow depth at the same pixel (y-axis). The black one-to-one line shows the modeled and measured snow depths coincide. The red regression line shows the optimal correlation of the point cloud. The Regression Line Slope (RLS), coefficient of determination (R^2) and Root Mean Square Error (RMSE) are three statistical values to describe the model precision. The color of the point cloud corresponds to the kernel density estimation (KDE) and shows the density of the point clouds.

6 Discussion

6.1 Relevant modeling parameters

The interpolated snow depths and SCD are the most important variables in the RF-model. These parameters give the model direct information about the snow depth and snow distribution. In contrast, the topographic variables contain indirect quantities about snow distribution in detailed spatial resolution. The SCD includes information about the snow distribution over the last six year. Therefore, it was expected that the SCD is a helpful variable for snow modeling because the RF-model searches for similarities between the years. I have not found a comparable variable like the SCD, which gives information about the temporal duration of snow cover, in the literature published so far. The interpolated snow depth is the only time bounded variable. Time bounded means that the interpolated snow depths contain time-dependent information about the snow depth in the observed region. The interpolated snow depths provide the RF-model with an indication snow amount at the modeled time compared to the time points of the training data. The high FI of interpolated snow depths indicates that a good automatized snow measurement network brings great advances in time-dependent snow modeling. In addition to interpolated snow depths (FI of 34%) and SCD (FI of 43%), the remaining 23% of FI is divided among five topographic variables. When looking at the FI for elevation, slope, aspect, TPI, or DAH individually, the FI seems very low but their sum contribute significantly to the RF-model.

Revuelto et al., 2020; Cartwright et al., 2022; Grünewald et al., 2013; López-Moreno et al., 2017; Daudt et al., 2022 also use the neighborhood-based curvature variable TPI. The large neighborhood region resulting from the radius analysis of the TPI is also used in similar proportion as the spatial resolution in Revuelto et al., 2020 and López-Moreno et al., 2017. By using the DAH, the slope and exposition lose some importance in the RF-model. The elevation and interpolated snow depths are directly integrated in the RF-model. Accordingly, the elevation variable loses some importance in the RF-model. The division of the FI shows that the decision tree nodes in the RF-model can be divided into three rough categories. The interpolated snow data represents the rough snow depth at the time considered, the SCD indicates the snow distribution of the past years and the topographic parameters show the location and its characteristics in the study area. The decision trees of the RF-model have a depth up to ten nodes. Accordingly, all three variable categories (interpolated snow depth, SCD and topographic variables) are involved in the snow depth modeling.

The parameter weight of the topographic variables changes slightly at different detailed spatial resolutions. The FI of the SCD decreases strongly at spatial resolutions of 50 m and 100 m. In contrast, the interpolated snow depths become more important for coarser spatial resolutions (Chapter 5.2.2). The FI of the SCD and interpolated snow depths differ greatly among model runs with a pixel length of 50 m (Figure 5.6). It has to be considered that the SCD has an original resolution of 10 m and the interpolated snow depths an original resolution of 20 m. The large variability of the FI at different modeled point over time could possibly come from topographic shapes which are no longer considered at a pixel length of 50 m. The interpolated snow depths base on the snow depth from the measurement stations and the DEM are strongly smoothed. Therefore, it was expected that coarser resolution of the already strongly smoothed interpolated snow depth leads to an increase of the FI. At the same time, the topographic details included in the SCD lose their deciding power. The topographic variables that show more detailed information at 6 m resolution do not become more important (Figure 5.6).

The FI differ more between the different study regions as with changing spatial resolution. The three study regions located in Davos (Davos, Latschüelfurgga and Schürlialp) have a more similar FI distribution than the study regions in the other Alpine areas (Laucherenalp, Berninapass, Saflischpass, Wägital) (Figure 5.7). The smaller FI of the interpolated snow depth in regions with one or two training data sets indicates that the variable of the interpolated snow depth mainly causes the temporal differences in the modeling. Since no temporal shift is trained in the RF-model when using only one training data set, it is comprehensible that the interpolated snow depth has a lower FI. At Laucherenalp and the Wägital, the FI for elevation is high compared to the other regions (Grünewald et al., 2014). This can be explained due to the one-sided topographic characteristics of these two regions. Figure 2.2 shows a regular distribution of the number of pixels over the elevations in the Wägital and Laucherenalp region. The large elevation difference in these comparatively small areas could be the reason of the high FI for elevation. Smaller topographic features as hollows or wind-exposed ridges are less dominant. This leads to a decrease of the FI for the TPI (Figure 5.7). The FI reflects the rough topographic characteristics of the study areas. The distribution of FI across variables depends on the training conditions of the RF-model, such as the size of the study area and the number of training data. With similar distribution of FI in different study regions, it is expected that the transferability of RF-model achieves high precision. Therefore, a training region topographically similar to the study region should be used.

The results of the FI analysis match well with the variable correlation analysis from Chapter 5.1.3. The stronger the correlation of the variable with the measured snow map, the more often the variable is used at the nodes of the decision trees in the RF-model. Therefore, the FI increases. It does not matter if there is a negative or positive correlation between the variable and the measured snow depths.

6.2 Variations of the model accuracy depending on the spatial resolution

The model precision statistically increases with coarser spatial resolution. The statistical values used do not show the added value that finer spatial resolutions present in the snow depth maps. The decrease of the R^2 value and the RMSE with coarser spatial resolutions (Figure 5.8), indicates a statistical improvement of the model precision with larger pixels. At the same time, the mean snow depth decreases for the measured and modeled snow depth maps (Figure 6.1). For example, the southern part of the Dischma valley (Figure 5.10) shows that small snow rich areas, an example is marked in the red circle, are still clearly visible with a coarse spatial resolution of 100 m. No variable in the RF-model gives information about the snow depth distribution from the training time points. No coordinates in the model are used which could localize snow accumulations in the considered region. The increased SCD in the red circle in Figure 5.10 indicates that this snow accumulation is modeled based on the SCD at all spatial resolutions.

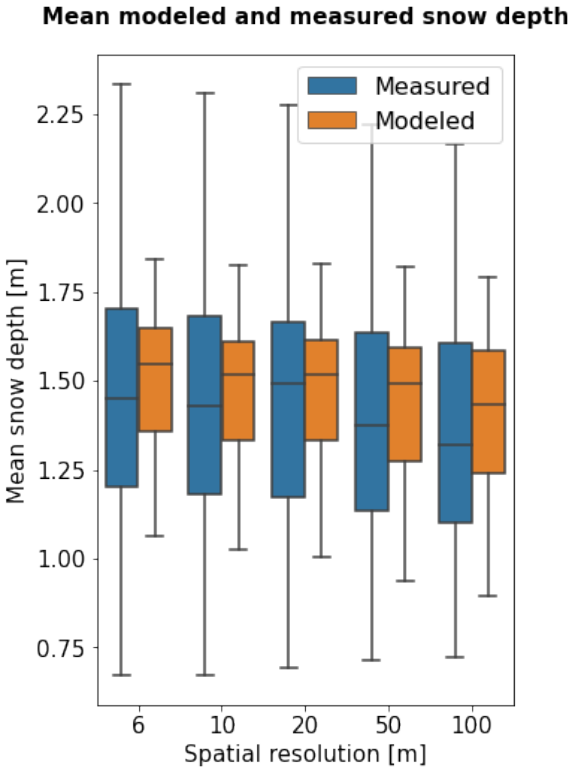

FIGURE 6.1: The box plot shows the snow depth averages comparing the measured and modeled snow maps. A box plot represents all 14 points of the Davos region. The breakdown into the different spatial resolutions shows a decrease of the mean snow depth with increasing pixel size. The length of the orange measured mean values indicate a stronger distribution at the different time points.

The restricted interval of the modeled snow depth at fine spatial resolution up to 20 m indicates an over-fitting of the strongly represented mean snow depths (scatter plot in Figure 5.10). Due to the increasing number of pixels with decreasing spatial resolution, the decision trees built during the training focus more on the numerous snow depths around the mean. The frequent snow depths are well modeled compared with the validation data. Therefore, the statistical coefficients (R^2, RMSE, MAE and MAD) are optimized. The RF-model training bases on achieving the best possible statistical values. Thus, the modeled snow depths are always too homogeneously distributed. At coarser resolutions (50 m or 100 m pixel length), less extreme deep snow depths are measured. This is due to merging small pixels together and take the mean. Merging pixels increases R^2 and decreases RMSE which says that the model precision

increases. Coarser spatial resolution does not increase the model precision but it smooths the extreme values which are hard to model. It depends on the research question if it is important that the model resolves the extreme values as it is needed to forecast avalanches or if the RF-model should predict the mean snow amount in a region as it is important for hydropower plants.

6.3 Temporal variations in snow depth distribution

The intra-annual analysis (Chapter 5.4) indicates that the RF-model trained at the snow peak times gives less precise results at other times during the season than a RF-model trained with data spreaded over the whole season. The modeled regression line is much steeper in October and December then in the second half of the snow season (Figure 5.11). This indicates a too heterogeneously modeled snow cover at the beginning of the snow season. The RF-model used for Latschüelfurgga and Schürlialp was trained with the Davos data recorded at the snow peak in March or April (marked red in Figure 5.11). The RLS of the other modeling times in spring (Figure 5.11) shows that the snow distribution of the RF-model corresponds well to the observed pattern. This agree with the mean analysis in Figure 6.1. The snow depth distribution per number of pixels peaks at low snow depth at the beginning of the snow season (histograms in Figure: 5.2, A.4 and A.7). Therefore, the snow is homogeneously distributed. Towards the end of the season, the snow distribution becomes more heterogeneous which leads to a broader histogram. The snow depth heterogeneity is a result of external processes as wind and irradiation due to the topographic variability. Because most of the training data are from the snow peak the RF-model has difficulties to model the homogeneous snow distribution at the beginning of the season.

The annually repeating similar spatial patterns of snow depth distribution justifies high model precision in inter-annual comparison. The RLS in the inter-annual analysis are mostly below one (Figure 5.12). This reflects the finding of too homogeneously modeled snow distribution which can be seen in the comparison of modeled and measured snow depth maps (Figure 5.10, 5.13, C.2, C.3 and C.1). Inter-annual modeling deviations are also evident in the R^2 values (Figure 5.9). The lower R^2 value in January 2016 may be due to the difference in modeling time compared to the training data, which are all based on the snow peak in March or April. The snow maps of the Davos region (Appendix A Figure A.5) shows the reduced snow amounts in January with a mean value of 0.72 m compared to the training data. The RF-model has difficulties to model the low snow winter 2022 precise. Therefore, the R^2 value is lower compared to other years (Figure 5.9). In the same year, the snow depth map covers a bigger area, especially in the southeast of the Davos region (Figure A.5). This area in the southeast is unknown for the RF-model. The RMSE in 2010 and 2019 differs from the other modeled time points (Figure 5.9). In these two years, the deviation of the mean values between the interpolated snow depths

and the area-wide measured snow depths are bigger than for the other years (Figure 5.3). A generally too small or too large amount of snow, which is implemented in the RF-model by the interpolated snow depths, causes large deviations in the unit-based RMSE. The 2010 modeling has an RMSE of 1.75 m at a spatial resolution of 20 m. This deviates strongly from the average RMSE of 0.5 m at identical spatial resolution. This shows that the relation between the interpolated snow depths of the stations and the measured snow amounts is enormously important. The RF-model is less precise in modeling extreme seasonality and climatic conditions like snowy winters (2010) or low snow seasons (2022). In such extreme seasons, the measured snow depth distribution differ strongly from the training data which leads to higher modeling uncertainties. Therefore, it is even more important that large and diverse snow depth maps are integrated into the training data.

The application of a snow depth model in areas that are not included in the training region is one of the main goals of the RF-model. Grünewald et al., 2013 and Revuelto et al., 2020 point out difficulties in the spatial extrapolation of their snow models. The four considered regions Wägital, Laucherenalp, Saflischpass and Berninapass as well as the reference region Davos North show how different the model precision is depending on the topographic properties.

The R^2 and RMSE values show how differently precise the RF-model can predict the snow distribution in the validation regions. The R^2 values from the Wägital (0.3) and the Laucherenalp (0.28) are particularly low and the RMSE is high (Wägital, 1.62 m and Laucherenalp, 1.7 m) (Table 5.3). Both, the low R^2 and the high RMSE indicate an imprecise modeling of the Wägital and Laucherenalp. The measured and modeled snow maps as well as its difference between measured and modeled snow maps from the Wägital (Figure C.2) and the Laucherenalp (Figure C.3) show the dependence of the snow depth on the elevation. The FI (Figure 5.7) indicates a somewhat greater influence of elevation in the modeled regions Wägital and Laucherenalp compared to the training region Davos. The many positive difference values (measured - modeled) suggest the underestimation of the snow depth in the model (Figure C.2). This could be due to the interpolation of snow depths from the stations or due to the few overlapping elevations between the training region Davos and the Wägital (Figure 2.2). General differences in topography between training and validation regions may lead to uncertainties in the spatial extrapolation of the RF-model.

The RF-model is able to model the two more topographically more diverse regions (Saflischpass and Berninapass) more precisely compared to the two slope-oriented regions (Laucherenalp and Wägital). The R^2 values for the Saflischpass (0.51) and for the Berninapass (0.42) are higher than for the reference region Davos North (0.4). This indicates that the spatial distance to the training area has no direct influence on the model precision in this setup. It should be taken into account that by dividing the large Davos region into sub-regions, the training region is reduced in size. The RMSE of the Saflischpass is with 1.58 m very high. The snow depth map

of the Saflischpass (Figure C.1 b) shows the heterogeneous snow distribution in the topographically diverse area. The RF-model models a too homogeneous snow distribution (Figure C.1 a and d) which can lead to an increased RMSE. Figure C.1 c shows that the measured small-scale differences can not be reproduced by the RF-model. The potential of the RF-model is shown by the scatter plot of the Berninapass (Figure 5.13 d). Most points are located near the one-to-one line. Like for Saflischpass, the RF-model models a too homogeneous snow distribution for the Berninapass. The snow-filled gullies and blown ridges are still evident in the modeled snow map (Figure 5.13 a) but less clear than in the measured snow map (Figure 5.13 b).

The RF-model precision depends on the topographic difference between training and validation regions. Large and variable training regions can generate a more diverse RF-model structure and thus produce better results in unknown regions. Compared to Revuelto et al., 2020 who uses an RF-model trained with terrestrial laser scanner (TLS) snow depth maps, the airborne snow depth maps used for this work cover a more than 300 times larger training region. The stronger the unknown applying region differ form the training region the more demanding it is to achieve a precise model result.

6.4 Random Forest for snow depth modeling: Advances and limitations

The statistical values (R^2 and RMSE) are similar to other snow models. Revuelto et al., 2020 uses an analog RF-model and a spatial resolution of 1 m. The authors end up with a model precision of: maximum R^2 value of 0.73, a MAE of 0.56 m and MAD of 0.52 m. Compared to Revuelto et al., 2020, the spatial resolution for this work is higher (6 m) and the study area 300 times bigger. Therefore, RF-model precision is slightly lower: average R^2 values of 0.41, MAE of 0.6 m and MAD of 0.5 m.

Grünewald et al., 2013 modulates with a multiple linear regression approach a test region near Davos with a spatial resolution of 100 m to 800 m pixel width. The R^2 values range from 0.4 to 0.8 with increasing spatial resolution. With an average R^2 value of 0.56 at a pixel width of 100 m, the RF-model presented in this work is statistically better in modeling the snow distribution. The Davos region is much larger then the study area from Grünewald et al., 2013. Both study regions are similar in terms of topographic difficulty due to its close location. As me, Grünewald et al., 2013 also identifies larger R^2 values with increasingly coarse spatial resolution (Figure 5.8). The comparison of absolut statistical values between snow depth models is difficult due to the big differences in model setup like differences in the topography of the study area, reference data, spatial and temporal resolution and size of model area.

The comparison with other snow depth models shows that the RF-model achieves similar precision. Zheng et al., 2016 reach R^2 values of 0.27 with a linear regression approach. Grünewald et al., 2013 models a precision of R^2 0.46 with a multiple linear regression model. The R^2 of Grünewald et al., 2013 vary strongly between different study regions. The model precision of the RF-model presented here reaches an average R^2 value of 0.56. Accordingly, an ML-based approach such as the RF principle is a suitable method for modeling snow distributions.

A temporal extension of the snow depth distribution over a snow season is difficult to model with the RF-model (Figure 5.11). To model at the beginning of the snow season as well as during the melting period, the RF-model must be trained with training data from the different points in time.

The modeling of areas with heavy vegetation or urban regions is not investigated. Luo et al., 2022 dealt in more detail with the modeling of snow in forested regions. In this work, urban and forested areas were masked out by generous masking (Chapter 3.1.2).

A homogenized distribution of snow in contrast to the measured snow map is a common problem in modeling. The RF-model distributes the snow amounts more regularly in the study area than desired (Figure 5.10, 5.13, C.1, C.2 and C.3). Topographic subtleties with snow filled grooves and blown off edges are only partially reproduced by the modeling. However, the increase in snow volume at higher altitudes becomes more important. The mean snow depths of the individual models are closer together than the mean snow depths of the 14 measured snow maps (Figure 6.1). Due to the model settings, the RF-model results never show areas with no snow. For all modeled surfaces, a snow depth will inevitably result. Whether the surface is covered with snow at all under the respective circumstances would have to be calculated in a preliminary step.

The RF-principle has been proven as a snow modeling basis (Hu et al., 2021; Cartwright et al., 2022; Revuelto et al., 2020). The large amount of data used to build the model during the training process includes many combinations of topographic parameters. Thus, by using larger training regions and snow maps from different points in time, a diverse and stable model can be built. Since only a few regions have such precise snow maps as the Davos region, one goal of snow modeling is to apply the model to new regions. The local statistical model of Grünewald et al., 2013, which is also used in the Swiss Alps, reaches its limit when extrapolating the trained model. Also Revuelto et al., 2020 with the very similar RF-model trained in high spatial resolution but on small areas has a mean RMSE of more than 0.8 m, which is significantly higher than the model precision in the same region. The RMSE values of the five regions used for transferability are between 0.4 m and 1.6 m, indicating that the model is not able to model at the same precision in all regions. Bigger elevation ranges in the training data reduces the model precision.

7 Conclusion and Outlook

7.1 Conclusion

The topographically diverse and large-scale study region of Davos makes the RF-model robust and flexible in its application. The snow depth modeling approaches and help to quantify the water stored in the snow (SWE) and therefore to answer key questions in water and risk management. The snow depth maps resulting from the RF-model can be used to understand the formation and dynamics of snow avalanches, for flood hazards or estimation of the available water for hydropower generation. In the following, the answer to the four research questions regarding parameter weighting, varying spatial resolution, an inter- and intra-annual comparison, as well as the transferability of the RF-model are summarized.

Combined, the topographic variables contribute similarly to the RF-model decision as the interpolated snow depths and SCD separately. The SCD and the interpolated snow depths of the measuring stations give direct information about the snow amounts in contrast to the topographic variables. Despite the limitations of the spatial resolution which is limited to 10 m for the SCD and 20 m for the interpolated snow depths, these two variables are used most intensively for decision making even on a detailed spatial resolution. Above a spatial resolution of ≥ 50 m, the Feature Importance (FI) of the interpolated snow depths gains significantly at the expense of the SCD. Above a spatial resolution of 50 m, the elevation difference exerts an increasingly larger influence on the snow distribution than fine-scale topographic changes. Unlike other snow depth models (Revuelto et al., 2020; Cartwright et al., 2022; Daudt et al., 2022), the included SCD is new and very effective considering its high FI. Furthermore, the use of daily interpolated snow depths makes this approach significantly different from previous snow depth models.

The R^2 values of the model accuracy increase from 0.41 to 0.56 with a resolution adjustment from 6 m to 100 m. This indicates that model precision increases with larger pixels size. The more detailed spatial resolution brings the problem that the extremes of low and high snow depths are hardly modeled by the RF-model. The increasing amount of data with higher resolutions becomes so large that the majority of pixels around the mean snow depth, shape most decision trees. The results of the snow depth map are also convincing in the more detailed spatial resolution up to 6 m pixel size. The published snow depth models work with different spatial resolutions (Revuelto et al., 2020; Daudt et al., 2022; López-Moreno et al., 2017; Cartwright et al., 2022). Often, the spatial resolution is determined based on the available data. Although

some of the data used here would be available at resolutions from 10 cm to 2 m, the limited computational capacity and imprecise modeling makes it unattractive to exploit the maximum degree of detail in the data. The visual comparison of measured to modeled snow depth map shows that fine spatial patterns are partly well modeled in the range of pixel lengths between 6 m and 20 m. It is important to adjust the spatial resolution to the final application of the snow depth map.

Due to the annually repeating snow distribution patterns, the RF-model models the snow distribution with high precision based on training data from other years. We tested the interannual relationship between the training and validation time points at the snow peak during the season. This study with 14 recordings at the snow peak in March or April each year shows that snow modeling has lower model precision in extremely low snow years or high snow years. The interpolated station data, which represents the absolute amount of snow in the model, cannot fully cover these large or small amounts of snow in the RF-model.

A larger temporal difference in the snow season between training and validation data reduces the model precision. Unknown time points at the beginning of the snow season are modeled too heterogeneously. Seasonal differences in snow depth modulation are hardly discussed in the literature.

The extrapolation of snow depth models was already attempted by Revuelto et al., 2020 and Grünewald et al., 2013 with limited success. Due to the large and diverse training area of the Davos region, only a slightly lower model precision could be achieved in two other Alpine regions than in the already known Davos region. In two other regions of the Alps, the modeling showed significantly worse statistical results. This shows that in the region used for the transferability, the threshold values and their distribution should lie within the interval of the training region. The RF-model is limited to trained snow depth values which makes it hardly possible to extrapolate beyond their limits.

The snow depth model developed in this thesis relies primarily on snow cover duration and interpolated snow depths. In application, the RF-model is bound to the training data times at the approximate times in the snow season. The good spatial extrapolation of the RF-model allows a flexible application in different alpine regions. Jonas et al., 2009 computes the SWE from snow depth only. The modeled snow depth maps of the RF-model, brings area-wide snow depth information to the calculation of SWE. The SWE of an inflow area can estimate the available capacity for reservoir operators. The distribution of snow amounts from the RF-model resulting map has a detailed spatial resolution and gives therefore specific information about avalanche situation on interested slopes.

7.2 Outlook

The potential of the RF-model is far from being exhausted. To improve the intra-annual modeling, a temporal variable could be integrated in the model. This should help the RF-model to know how the snow distribution generally should be. Therefore, the snow distribution during the season should be analyzed in more detail which requires data sets at different times during the snow season at detailed spatial resolution.

To achieve a heterogeneous snow distribution, the RF-model should be less focused on the mean. The number of pixels with similar topographic conditions in the training area should be distributed as evenly as possible. If enough training data is available, the topographic features could be grouped together. Frequent combinations are limited, so that a possible equal distribution of the topographic feature groups is created. This should lead to a higher model precision in areas with extreme snow depths.

Broxton et al., 2019 studied snow cover in forested areas. To obtain a comprehensive snow depth map, the inclusion of vegetation is essential. Insights from snow-covered vegetation areas could be integrated into the RF-model through a land cover map which was tried by Cartwright et al., 2022. This approach enable the RF-model to outperform snow modeling in heavily vegetated regions.

The RF-model developed in this thesis can estimate snow depths but is not able to model snow cover. In a further step, the model could learn where snow is located based on the interpolated snow depths or other temporal weather data.

The successful implementation of the gauging stations data have a great effect on the model accuracy. The snow depth from the measurement stations prevent a direct snow depth prediction. In a further step, future modeling of point snow depths can serve as basis for the RF-model for predicting snow volumes in the region of interest. These forward-looking capabilities of the RF-model are important for satisfying the applications of the snow depth maps. The RF-model offers the possibility to estimate region-specific snow volumes based on future climatic scenarios. Hydroelectric power plants could determine the melt capacity for energy production. On a larger scale, such snow distributions can also be used to estimate irrigation and drinking water reserves in the future.

Bibliography

Archer, D and D Stewart (1995). "installation and use of a snow pillow to monitor snow water equivalent." *Water and environmental management: journal of the Institution of Water and Environmental Management*.

Asuero, A. G., A. Sayago, and A. González (2006). "The correlation coefficient: An overview." *Critical reviews in analytical chemistry* 36.1, pp. 41–59.

Begert, M., T. Schlegel, and W. Kirchhofer (2005). "Homogeneous temperature and precipitation series of Switzerland from 1864 to 2000." *International Journal of Climatology: A Journal of the Royal Meteorological Society* 25.1, pp. 65–80.

Biau, G. and E. Scornet (2016). "A random forest guided tour." *Test* 25.2, pp. 197–227.

Böhner, J. and O. Antonić (2009). "Land-surface parameters specific to topo-climatology." *Developments in soil science* 33, pp. 195–226.

Breiman, L. (2001). "Random forests." *Machine learning* 45.1, pp. 5–32.

Broxton, P. D., W. J. Van Leeuwen, and J. A. Biederman (2019). "Improving snow water equivalent maps with machine learning of snow survey and lidar measurements." *Water Resources Research* 55.5, pp. 3739–3757.

Bühler, Y, M Marty, L Egli, J Veitinger, T Jonas, P Thee, and C Ginzler (2015). "Snow depth mapping in high-alpine catchments using digital photogrammetry." *The Cryosphere* 9.1, pp. 229–243.

Bühler, Y., M. S. Adams, R. Bösch, and A. Stoffel (2016). "Mapping snow depth in alpine terrain with unmanned aerial systems (UASs): potential and limitations." *The Cryosphere* 10.3, pp. 1075–1088.

Bühler, Y., L Meier, and C. Ginzler (2014). "Potential of operational high spatial resolution near-infrared remote sensing instruments for snow surface type mapping." *IEEE Geoscience and Remote Sensing Letters* 12.4, pp. 821–825.

Bührle, L. J., M. Marty, L. A. Eberhard, A. Stoffel, E. D. Hafner, and Y. Bühler (2022). "Spatially continuous snow depth mapping by airplane photogrammetry for annual peak of winter from 2017 to 2021." *The Cryosphere Discussions*, pp. 1–37.

Bühler, Y., L. Bührle, L. Eberhard, M. Marty, and A. Stoffel (Oct. 2021). "Grossflächige Schneehöhen-Kartierung mit Flugzeug und Satellit." *Geomatik* 119, pp. 213 –215.

Cartwright, K., C. Mahoney, and C. Hopkinson (2022). "Machine learning based imputation of mountain snowpack depth within an operational Lidar sampling framework in Southwest Alberta." *Canadian Journal of Remote Sensing* 48.1, pp. 107–125.

Daudt, R. C., H. Wulf, E. D. Hafner, Y. Bühler, K. Schindler, and J. D. Wegner (2022). "Snow depth Estimation at Country-Scale with High Spatial and Temporal Resolution." *ISPRS Journal of Photogrammetry and Remote Sensing*.

De Reu, J., J. Bourgeois, M. Bats, A. Zwertvaegher, V. Gelorini, P. De Smedt, W. Chu, M. Antrop, P. De Maeyer, P. Finke, et al. (2013). "Application of the topographic position index to heterogeneous landscapes." *Geomorphology* 186, pp. 39–49.

Di Marco, N., D. Avesani, M. Righetti, M. Zaramella, B. Majone, and M. Borga (2021). "Reducing hydrological modelling uncertainty by using MODIS snow cover data and a topography-based distribution function snowmelt model." *Journal of Hydrology* 599, p. 126020.

Eberhard, L., M. Marty, A. Stoffel, R. Kenner, and Y. Bühler (2018). "Photogrammetric snow depth mapping: Evaluation of different plant-forms and sensors."

Eberhard, L. A., P. Sirguey, A. Miller, M. Marty, K. Schindler, A. Stoffel, and Y. Bühler (2021). "Intercomparison of photogrammetric platforms for spatially continuous snow depth mapping." *The Cryosphere* 15.1, pp. 69–94.

Farinotti, D., S. Usselmann, M. Huss, A. Bauder, and M. Funk (2012). "Runoff evolution in the Swiss Alps: Projections for selected high-alpine catchments based on ENSEMBLES scenarios." *Hydrological Processes* 26.13, pp. 1909–1924.

Fassnacht, S., K. Dressler, and R. Bales (2003). "Snow water equivalent interpolation for the Colorado River Basin from snow telemetry (SNOTEL) data." *Water Resources Research* 39.8.

Fierz, C., R. L. Armstrong, Y. Durand, P. Etchevers, E. Greene, D. M. McClung, K. Nishimura, P. K. Satyawali, and S. A. Sokratov (2009). "The international classification for seasonal snow on the ground."

Gleason, K. E., A. W. Nolin, and T. R. Roth (2017). "Developing a representative snow-monitoring network in a forested mountain watershed." *Hydrology and Earth System Sciences* 21.2, pp. 1137–1147.

Golding, D. L. (1974). "The correlation of snowpack with topography and snowmelt runoff on Marmot Creek Basin, Alberta." *Atmosphere* 12.1, pp. 31–38.

Grünewald, T., Y. Bühler, and M. Lehning (2014). "Elevation dependency of mountain snow depth." *The Cryosphere* 8.6, pp. 2381–2394.

Grünewald, T., J. Stötter, J. W. Pomeroy, R. Dadic, I. Moreno Baños, J Marturià, M. Sproß, C. Hopkinson, P. Burlando, and M. Lehning (2013). "Statistical modelling of the snow depth distribution in open alpine terrain." *Hydrology and Earth System Sciences* 17.8, pp. 3005–3021.

Hu, Y., T. Che, L. Dai, and L. Xiao (2021). "Snow depth fusion based on machine learning methods for the Northern Hemisphere." *Remote Sensing* 13.7, p. 1250.

Jonas, T., C. Marty, and J. Magnusson (2009). "Estimating the snow water equivalent from snow depth measurements in the Swiss Alps." *Journal of Hydrology* 378.1-2, pp. 161–167.

Kulakowski, D., P. Bebi, and C. Rixen (2011). "The interacting effects of land use change, climate change and suppression of natural disturbances on landscape forest structure in the Swiss Alps." *Oikos* 120.2, pp. 216–225.

Laternser, M. and M. Schneebeli (2003). "Long-term snow climate trends of the Swiss Alps (1931–99)." *International Journal of Climatology: A Journal of the Royal Meteorological Society* 23.7, pp. 733–750.

Liaw, A., M. Wiener, et al. (2002). "Classification and regression by randomForest." *R news* 2.3, pp. 18–22.

Liston, G. E., R. B. Haehnel, M. Sturm, C. A. Hiemstra, S. Berezovskaya, and R. D. Tabler (2007). "Simulating complex snow distributions in windy environments using SnowTran-3D." *Journal of Glaciology* 53.181, pp. 241–256.

López-Moreno, J. I., J. Revuelto, E Alonso-González, A. Sanmiguel-Vallelado, S. R. Fassnacht, J. Deems, and E. Moran-Tejeda (2017). "Using very long-range terrestrial laser scanner to analyze the temporal consistency of the snowpack distribution in a high mountain environment." *Journal of Mountain Science* 14.5, pp. 823–842.

Louppe, G., L. Wehenkel, A. Sutera, and P. Geurts (2013). "Understanding variable importances in forests of randomized trees." *Advances in neural information processing systems* 26.

Lowe, D. G. (2004). "Distinctive image features from scale-invariant keypoints." *International journal of computer vision* 60.2, pp. 91–110.

Luo, J., C. Dong, K. Lin, X. Chen, L. Zhao, and L. Menzel (2022). "Mapping snow cover in forests using optical remote sensing, machine learning and time-lapse photography." *Remote Sensing of Environment* 275, p. 113017.

Marti, R., S. Gascoin, E. Berthier, M De Pinel, T. Houet, and D. Laffly (2016). "Mapping snow depth in open alpine terrain from stereo satellite imagery." *The Cryosphere* 10.4, pp. 1361–1380.

McGrath, D., R. Webb, D. Shean, R. Bonnell, H.-P. Marshall, T. H. Painter, N. P. Molotch, K. Elder, C. Hiemstra, and L. Brucker (2019). "Spatially extensive ground-penetrating radar snow depth observations during NASA's 2017 SnowEx campaign: Comparison with In situ, airborne, and satellite observations." *Water Resources Research* 55.11, pp. 10026–10036.

Mendoza, P. A., K. N. Musselman, J. Revuelto, J. S. Deems, J. I. López-Moreno, and J. McPhee (2020). "Interannual and seasonal variability of snow depth scaling behavior in a subalpine catchment." *Water Resources Research* 56.7, e2020WR027343.

Miles, J. (2005). "R-squared, adjusted R-squared." *Encyclopedia of statistics in behavioral science*.

Nasim, S., M. Oussalah, B. Klöve, and A. T. Haghighi (2022). "Machine learning model for snow depth estimation using a multisensory ubiquitous platform." *Journal of Mountain Science* 19.9, pp. 2506–2527.

Nolan, M., C. Larsen, and M. Sturm (2015). "Mapping snow depth from manned aircraft on landscape scales at centimeter resolution using structure-from-motion photogrammetry." *The Cryosphere* 9.4, pp. 1445–1463.

Pedregosa, F., G. Varoquaux, A. Gramfort, V. Michel, B. Thirion, O. Grisel, M. Blondel, P. Prettenhofer, R. Weiss, V. Dubourg, J. Vanderplas, A. Passos, D. Cournapeau, M. Brucher, M. Perrot, and E. Duchesnay (2011). "Scikit-learn: Machine Learning in Python." *Journal of Machine Learning Research* 12, pp. 2825–2830.

Revuelto, J., P. Billecocq, F. Tuzet, B. Cluzet, M. Lamare, F. Larue, and M. Dumont (2020). "Random forests as a tool to understand the snow depth distribution and its evolution in mountain areas." *Hydrological Processes* 34.26, pp. 5384–5401.

Revuelto, J., J. I. López-Moreno, C. Azorin-Molina, J. Zabalza, G Arguedas, and S. M. Vicente-Serrano (2014). "Mapping the annual evolution of snow depth in a small catchment in the Pyrenees using the long-range terrestrial laser scanning." *Journal of Maps* 10.3, pp. 379–393.

Schirmer, M, V Wirz, A Clifton, and M Lehning (2011). "Persistence in intra-annual snow depth distribution." *Part I: Measurements and Topographic Control, submitted to Water Resour. Res*.

Schweizer, J., J Bruce Jamieson, and M. Schneebeli (2003). "Snow avalanche formation." *Reviews of Geophysics* 41.4.

Segal, M. R. (2004). "Machine learning benchmarks and random forest regression."

Senese, A, M Maugeri, E Vuillermoz, C Smiraglia, and G Diolaiuti (2014). "Using daily air temperature thresholds to evaluate snow melting occurrence and amount on Alpine glaciers by T-index models: the case study of the Forni Glacier (Italy)." *The Cryosphere* 8.5, pp. 1921–1933.

Serreze, M. C., M. P. Clark, R. L. Armstrong, D. A. McGinnis, and R. S. Pulwarty (1999). "Characteristics of the western United States snowpack from snowpack telemetry (SNOTEL) data." *Water Resources Research* 35.7, pp. 2145–2160.

Stone, M. (1974). "Cross-validation and multinomial prediction." *Biometrika* 61.3, pp. 509–515.

Strobl, C., A.-L. Boulesteix, A. Zeileis, and T. Hothorn (2007). "Bias in random forest variable importance measures: Illustrations, sources and a solution." *BMC bioinformatics* 8.1, pp. 1–21.

Sturm, M. and J. Holmgren (2018). "An automatic snow depth probe for field validation campaigns." *Water Resources Research* 54.11, pp. 9695–9701.

Sturm, M. and A. M. Wagner (2010). "Using repeated patterns in snow distribution modeling: An Arctic example." *Water Resources Research* 46.12.

swisstopo (Mar. 2022). *swissALTI3D Das hoch aufgelöste Terrainmodell der Schweiz*. Bundesamt für Landestopografie swisstopo. www.swisstop.ch.

Trujillo, E., J. A. Ramírez, and K. J. Elder (2009). "Scaling properties and spatial organization of snow depth fields in sub-alpine forest and alpine tundra." *Hydrological Processes: An International Journal* 23.11, pp. 1575–1590.

Vionnet, V., I. Dombrowski-Etchevers, M. Lafaysse, L. Quéno, Y. Seity, and E. Bazile (2016). "Numerical weather forecasts at kilometer scale in the French Alps: Evaluation and application for snowpack modeling." *Journal of Hydrometeorology* 17.10, pp. 2591–2614.

Viviroli, D., H. H. Dürr, B. Messerli, M. Meybeck, and R. Weingartner (2007). "Mountains of the world, water towers for humanity: Typology, mapping, and global significance." *Water resources research* 43.7.

Weiss, A. (2001). "Topographic position and landforms analysis." *Poster presentation, ESRI user conference, San Diego, CA*. Vol. 200.

Wilson, J. P. and J. C. Gallant (2000). *Terrain analysis: principles and applications*. John Wiley & Sons.

Winstral, A, J Magnusson, M Schirmer, and T Jonas (2019). "The Bias-Detecting Ensemble: A New and Efficient Technique for Dynamically Incorporating Observations Into Physics-Based, Multilayer Snow Models." *Water Resources Research* 55.1, pp. 613–631.

Wirz, V, M Schirmer, S. Gruber, and M Lehning (2011). "Spatio-temporal measurements and analysis of snow depth in a rock face." *The Cryosphere* 5.4, pp. 893–905.

Zevenbergen, L. W. and C. R. Thorne (1987). "Quantitative analysis of land surface topography." *Earth surface processes and landforms* 12.1, pp. 47–56.

Zheng, Z, P. Kirchner, and R. Bales (2016). "Topographic and vegetation effects on snow accumulation in the southern Sierra Nevada: a statistical summary from lidar data." *The Cryosphere* 10.1, pp. 257–269.

A Appendix: Data analysis

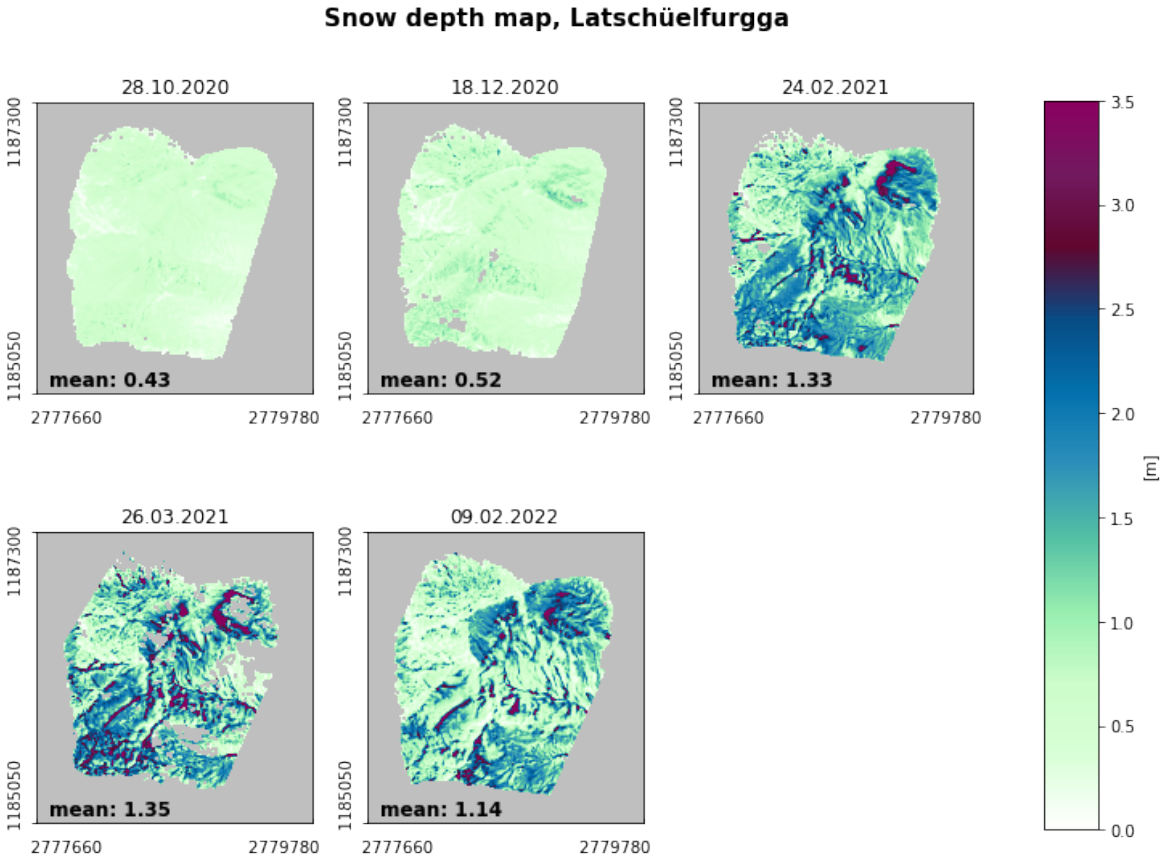

FIGURE A.1: Measured snow depth maps of the Latschüelfurgga study region. These measurements are based on the drone scans.

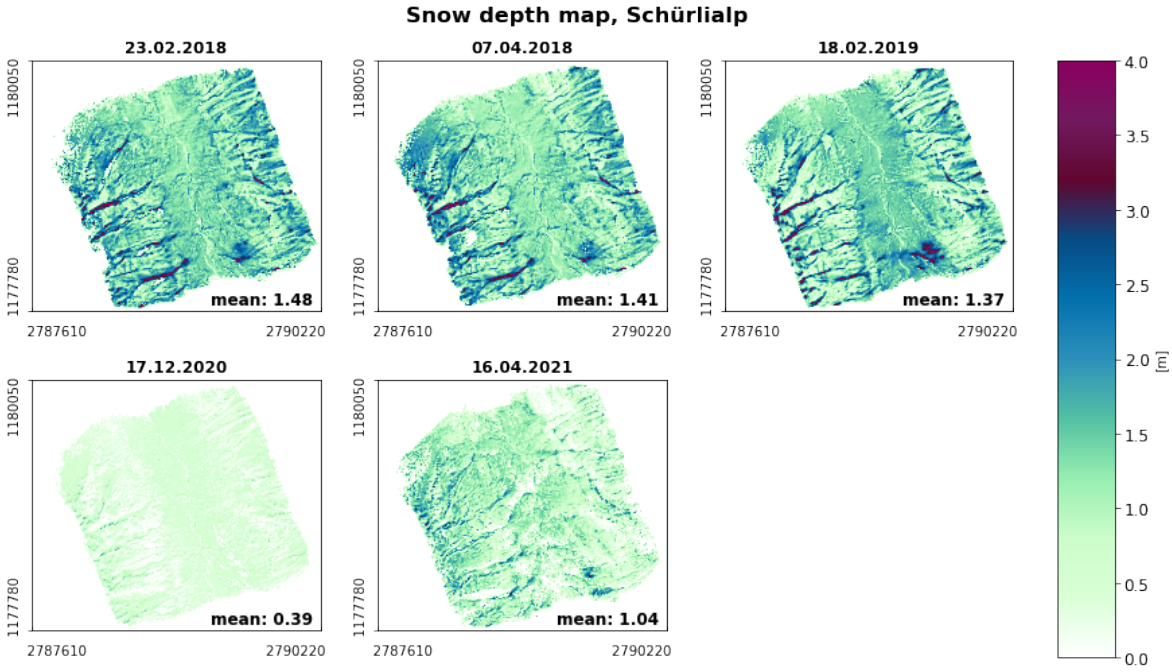

FIGURE A.2: Measured snow depth maps of the Schürlialp study region. These measurements are based on the drone scans.

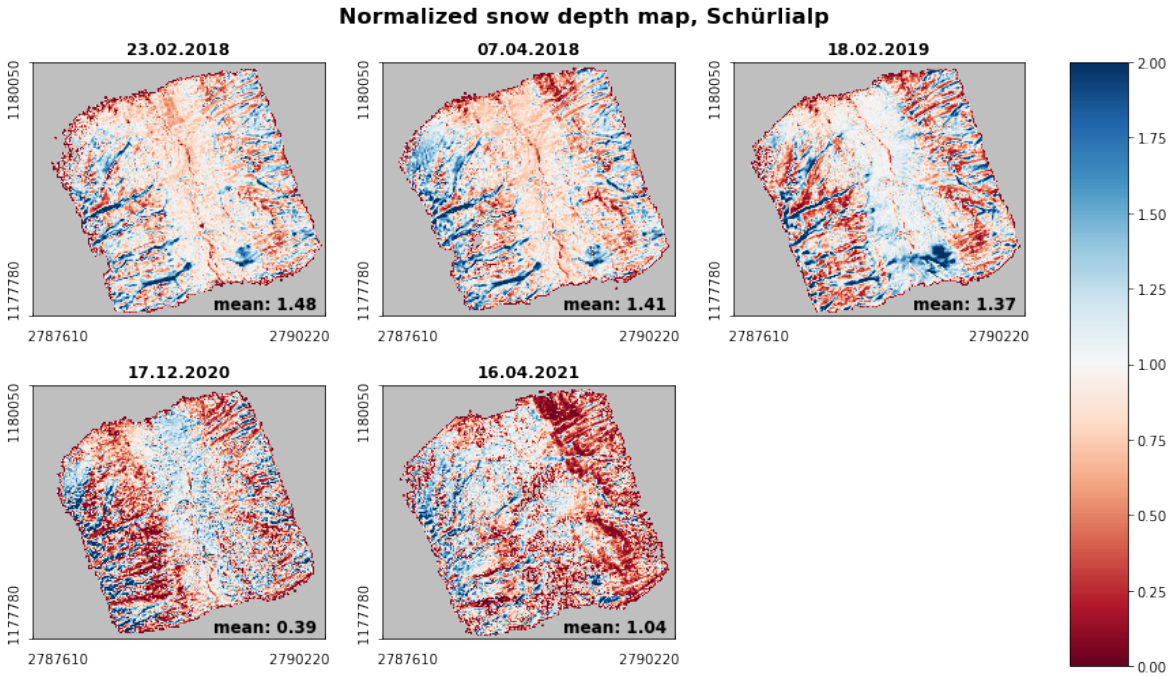

FIGURE A.3: Measured snow depth maps of the Schürlialp study region normalized by the mean snow depth. These measurements are based on the drone scans.

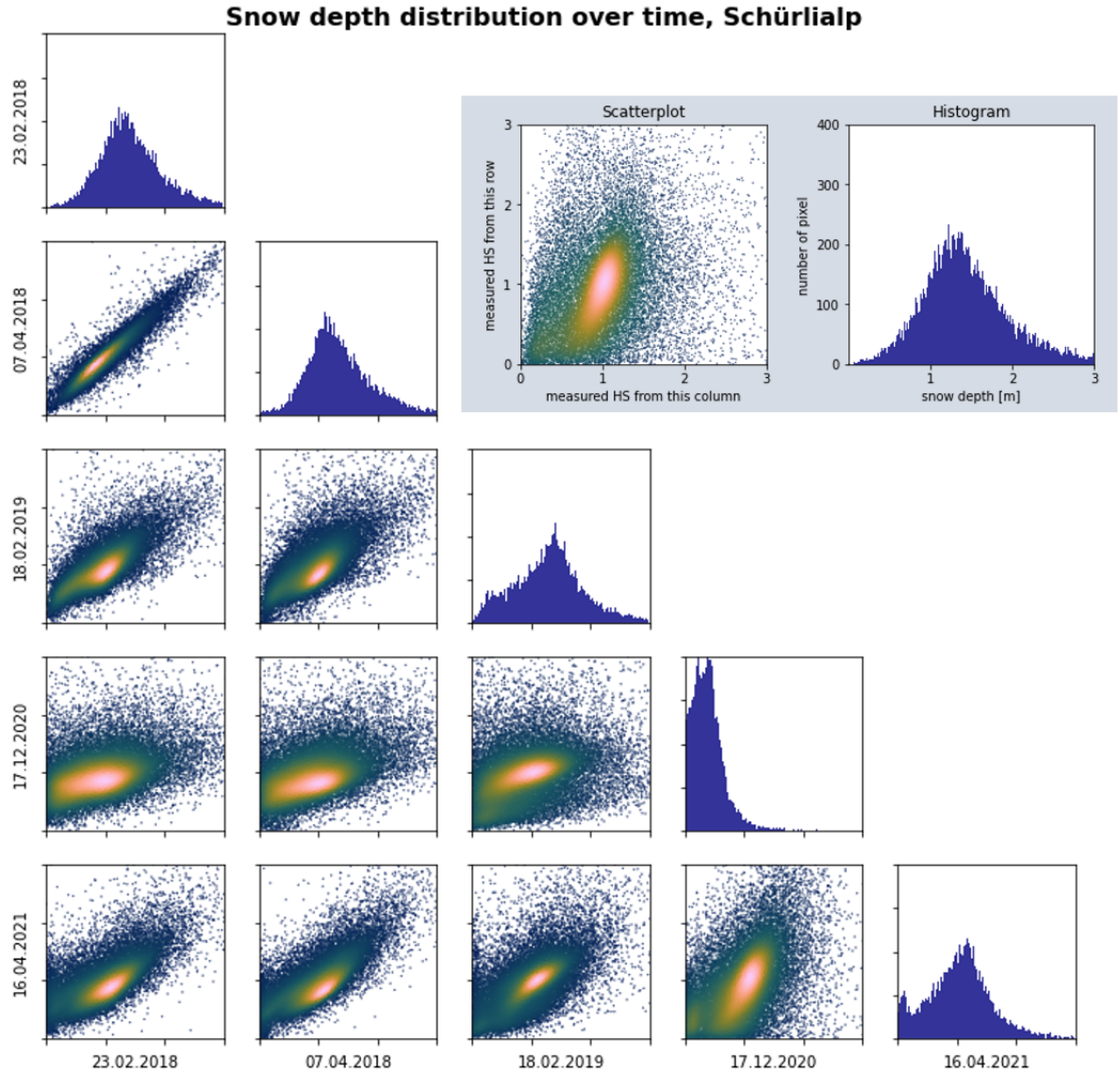

FIGURE A.4: The scatter plots show the pixel-by-pixel correlation analysis of snow depth maps. The axis information as well as the color legend of the kernel density estimation is in the gray box. The histograms show the distribution (y-axis) of the modeled snow depths in the (x-axis) respective snow depth map.

TABLE A.1: Statistical analysis of snow distribution from the five snow depth maps of the Schürlialp region. The R^2 values are in the lower left half of the table. Smaller R^2 values are colored in darker blue. A bigger (brighter colored) R^2 value describes a more similar distribution of snow at the two time points considered. The RMSE values are located at the top right of the table and are colored in darker green as the size increases. Smaller (brighter colored) RMSE values show more similar distribution of snow amounts at the two time points considered. A close correlation exists between the 23.02.2018 and 07.04.2018 snow maps.

	23.02.2018	**07.04.2018**	**18.02.2019**	**17.12.2020**	**16.04.2021**
23.02.2018		0.03	0.10	0.37	0.15
07.04.2018	0.87		0.13	0.34	0.12
18.02.2019	0.57	0.45		0.50	0.22
17.12.2020	0.19	0.25	-0.10		0.36
16.04.2021	0.44	0.57	0.21	-0.31	

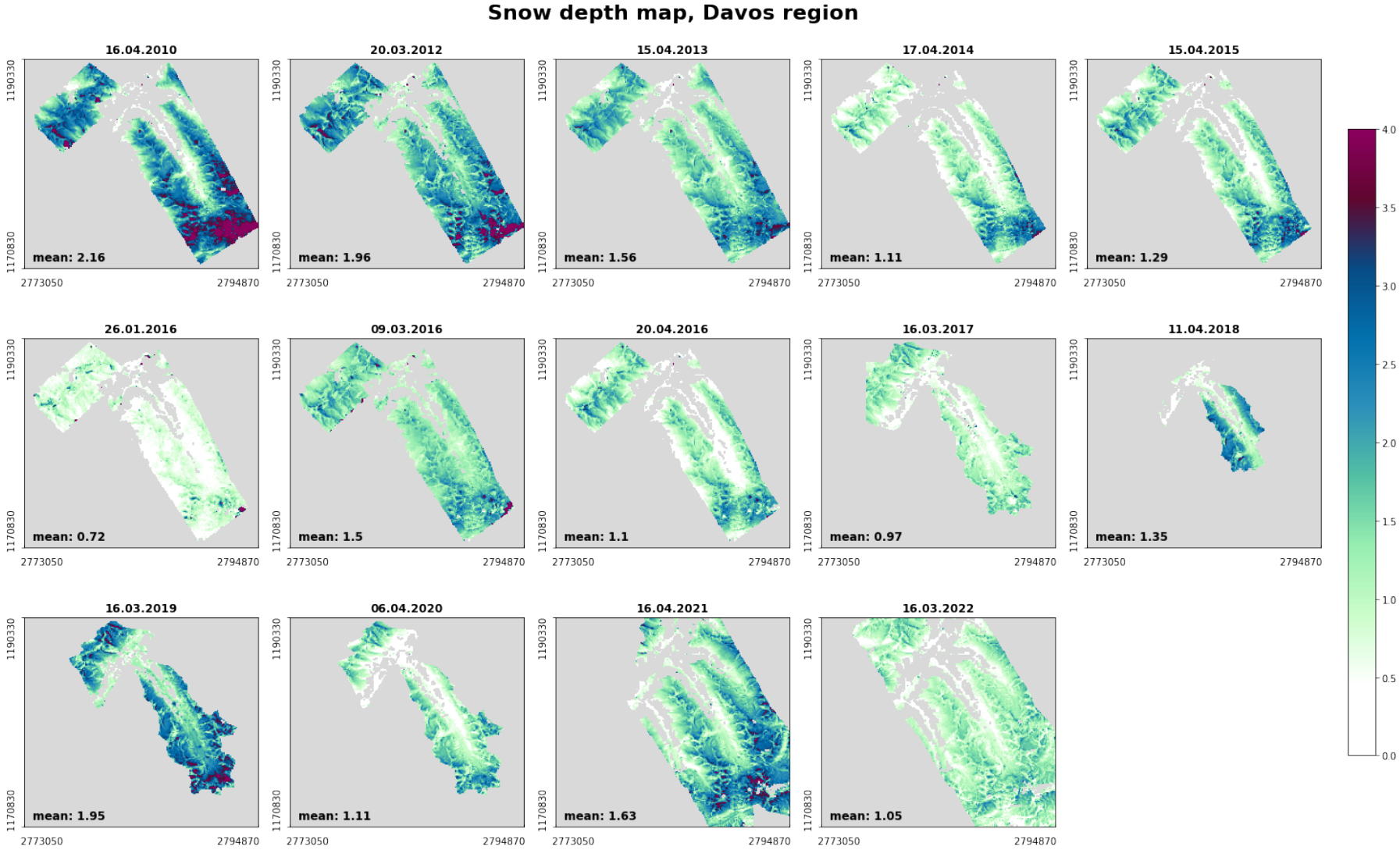

FIGURE A.5: Measured snow depth maps of the Davos region. These measurements are based on the airplane scans.

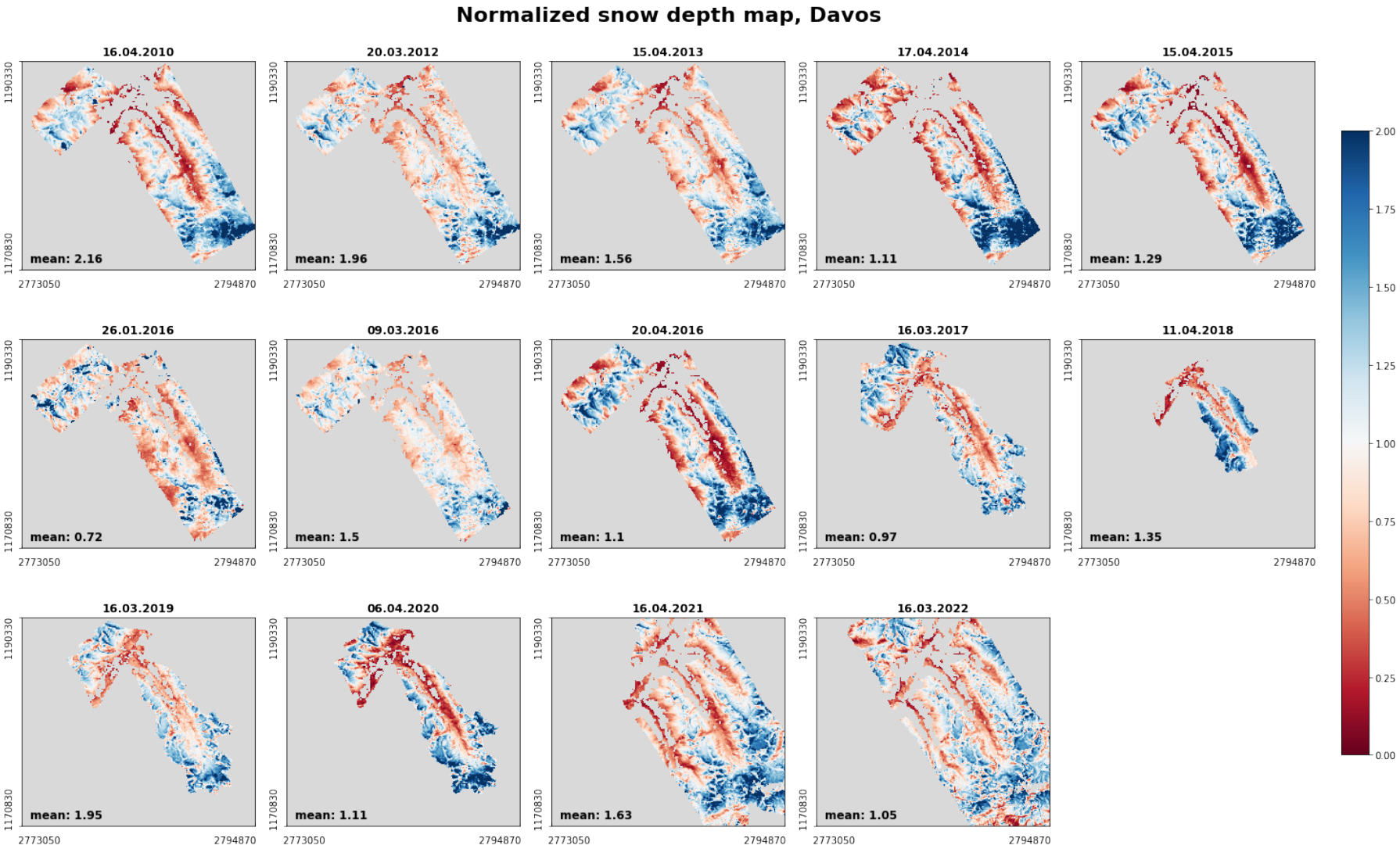

FIGURE A.6: Measured snow depth maps of the Davos region normalized with the mean snow depth from each point of time.

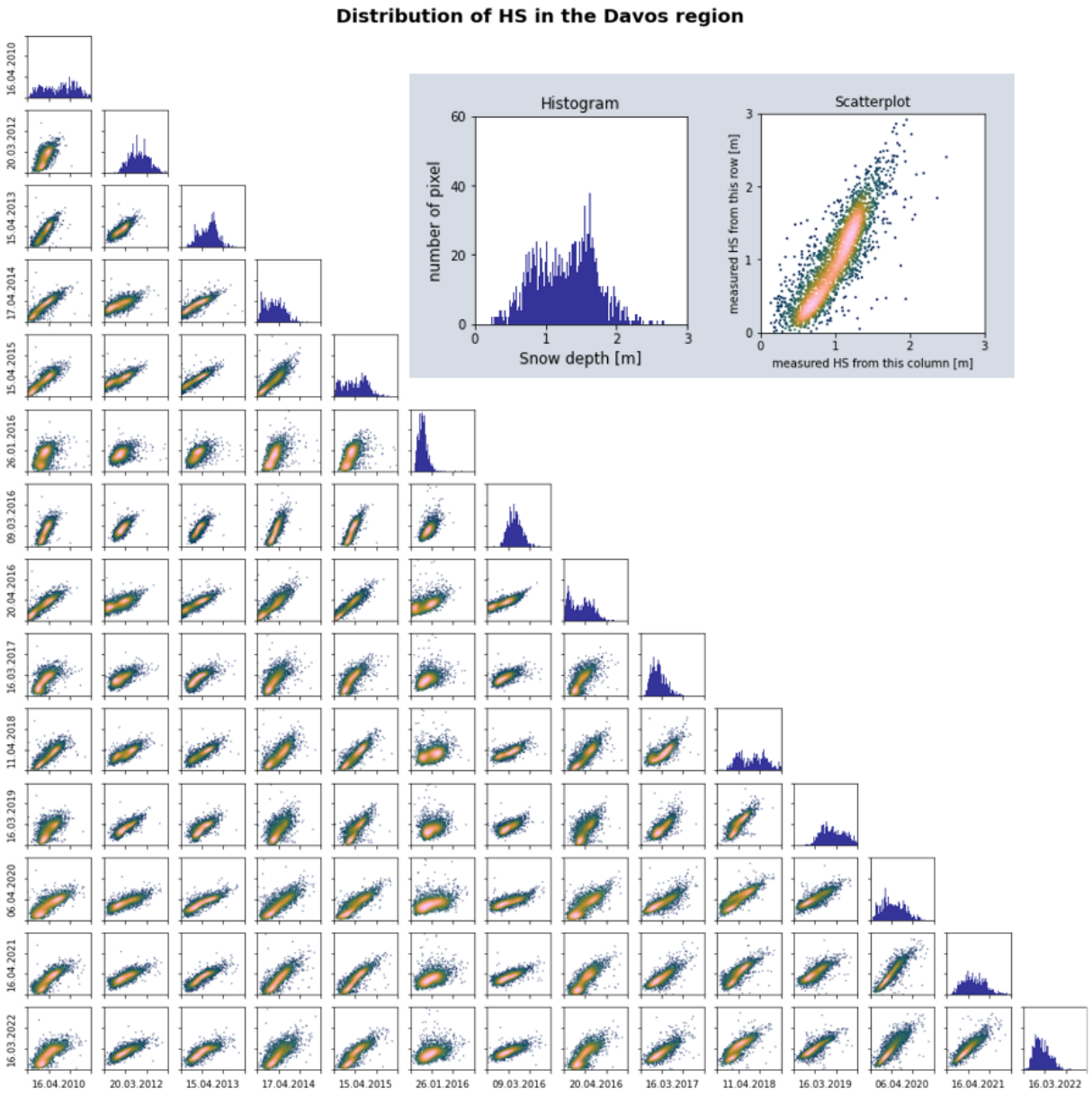

FIGURE A.7: The scatter plots show the pixel-by-pixel correlation analysis of snow depth maps. The axis information as well as the color legend of the kernel density estimation is in the gray box. The histograms show the distribution (y-axis) of the modeled snow depths in the (x-axis) respective snow depth map.

TABLE A.2: Statistical analysis of snow distribution from the five snow depth maps of the Davos region. The R^2 values are in the lower left half of the table. Smaller R^2 values are colored in darker blue. A bigger (brighter colored) R^2 value describes a more similar distribution of snow at the two time points considered. The RMSE values are located at the top right of the table and are colored in darker green as the size increases. Smaller (brighter colored) RMSE values show more similar distribution of snow amounts at the two time points considered.

	16.04.2010	**20.03.2012**	**15.04.2013**	**17.04.2014**	**15.04.2015**	**26.01.2016**	**09.03.2016**	**20.04.2016**	**16.03.2017**	**11.04.2018**	**16.03.2019**	**06.04.2020**	**16.04.2021**	**16.03.2022**
16.03.2022	0.17	0.10	0.11	0.16	0.13	0.23	0.11	0.17	0.10	0.07	0.06	0.07	0.05	
16.04.2021	0.13	0.10	0.09	0.13	0.12	0.23	0.11	0.15	0.10	0.06	0.07	0.05		0.75
06.04.2020	0.17	0.15	0.13	0.16	0.15	0.29	0.16	0.18	0.13	0.07	0.08		0.79	0.71
16.03.2019	0.17	0.07	0.09	0.19	0.15	0.22	0.08	0.20	0.09	0.05		0.69	0.58	0.67
11.04.2018	0.13	0.10	0.09	0.15	0.13	0.25	0.10	0.15	0.11		0.66	0.72	0.65	0.63
16.03.2017	0.10	0.06	0.06	0.11	0.09	0.15	0.06	0.11		0.56	0.57	0.62	0.63	0.60
20.04.2016	0.04	0.12	0.07	0.05	0.03	0.19	0.11		0.47	0.67	0.40	0.60	0.64	0.56
09.03.2016	0.08	0.03	0.03	0.09	0.09	0.09		0.65	0.42	0.53	0.42	0.51	0.53	0.52
26.01.2016	0.18	0.12	0.12	0.17	0.17		0.25	0.20	0.11	0.07	0.05	0.11	0.12	0.11
15.04.2015	0.04	0.08	0.05	0.04		0.19	0.70	0.84	0.54	0.74	0.56	0.73	0.73	0.71
17.04.2014	0.04	0.11	0.06		0.77	0.21	0.63	0.75	0.43	0.58	0.37	0.64	0.66	0.53
15.04.2013	0.05	0.03		0.71	0.78	0.17	0.62	0.73	0.49	0.66	0.51	0.69	0.72	0.60
20.03.2021	0.09		0.62	0.45	0.62	0.12	0.51	0.43	0.42	0.55	0.63	0.58	0.57	0.62
16.04.2010		0.44	0.71	0.76	0.77	0.12	0.55	0.78	0.41	0.69	0.39	0.62	0.66	0.50

B Appendix: Statistical values and Feature Importance of the RF-model

TABLE B.1: Statistical values (R^2, Median Absolute Deviation (MAD), Mean Absolute Error (MAE), Root Mean Square Error (RMSE)) of the model accuracy from snow modeling of the Davos region. All values are averaged over the 14 time points modeled using k-fold cross validation.

spatial resolution	R^2	MAD	MAE	RMSE
6 m	0.41	0.5	0.6	0.7
10 m	0.44	0.45	0.57	0.64
20 m	0.43	0.43	0.53	0.53
50 m	0.53	0.37	0.46	0.43
100 m	0.56	0.35	0.44	0.44

TABLE B.2: Feature Importance (FI) of the Davos region splited in different spatial resolution. Larger FI (in darker blue) represents more decision nodes in the decision trees of the RF-model.

spatial resolution	interp. HS	SCD	Elevation	Aspect	Slope	TPI	DAH
6 m	0.27	0.48	0.06	0.01	0.04	0.12	0.02
10 m	0.27	0.47	0.07	0.03	0.04	0.12	0.02
20 m	0.30	0.48	0.05	0.01	0.03	0.11	0.02
50 m	0.36	0.44	0.05	0.02	0.03	0.07	0.03
100 m	0.49	0.29	0.07	0.02	0.04	0.05	0.04

TABLE B.3: Regression Line Slope (RLS) of the Davos region at different spatial resolutions at the 14 time points modeled. RLS smaller than one (blue) indicates a too homogeneous distribution of snow amounts by the RF model. Too heterogeneously distributed snow amounts show an RLS greater than one (yellow-brown).

date	**6 m**	**10 m**	**20 m**	**50 m**	**100 m**
16.04.2010	0.539	0.642	0.5514	0.567	0.57
20.03.2012	0.742	0.749	0.768	0.793	0.806
15.04.2013	0.89	0.894	0.921	0.943	0.95
17.04.2014	1.025	1.044	1.088	1.153	1.156
15.04.2015	1.016	1.044	0.996	1.12	1.135
26.01.2016	0.897	0.903	0.935	0.891	0.858
09.03.2016	0.799	0.622	0.826	0.856	0.82
20.04.2016	0.916	0.928	0.964	0.994	0.995
16.03.2017	0.928	0.942	0.995	1.041	1.027
11.04.2018	0.699	0.706	0.726	0.758	0.767
16.03.2019	0.642	0.684	0.707	0.752	0.796
06.04.2020	1.058	1.08	1.134	1.2	1.228
16.04.2021	0.929	0.945	0.974	1.011	1.034
16.03.2022	0.923	0.993	0.908	0.882	1.12

C Appendix: Model transferability

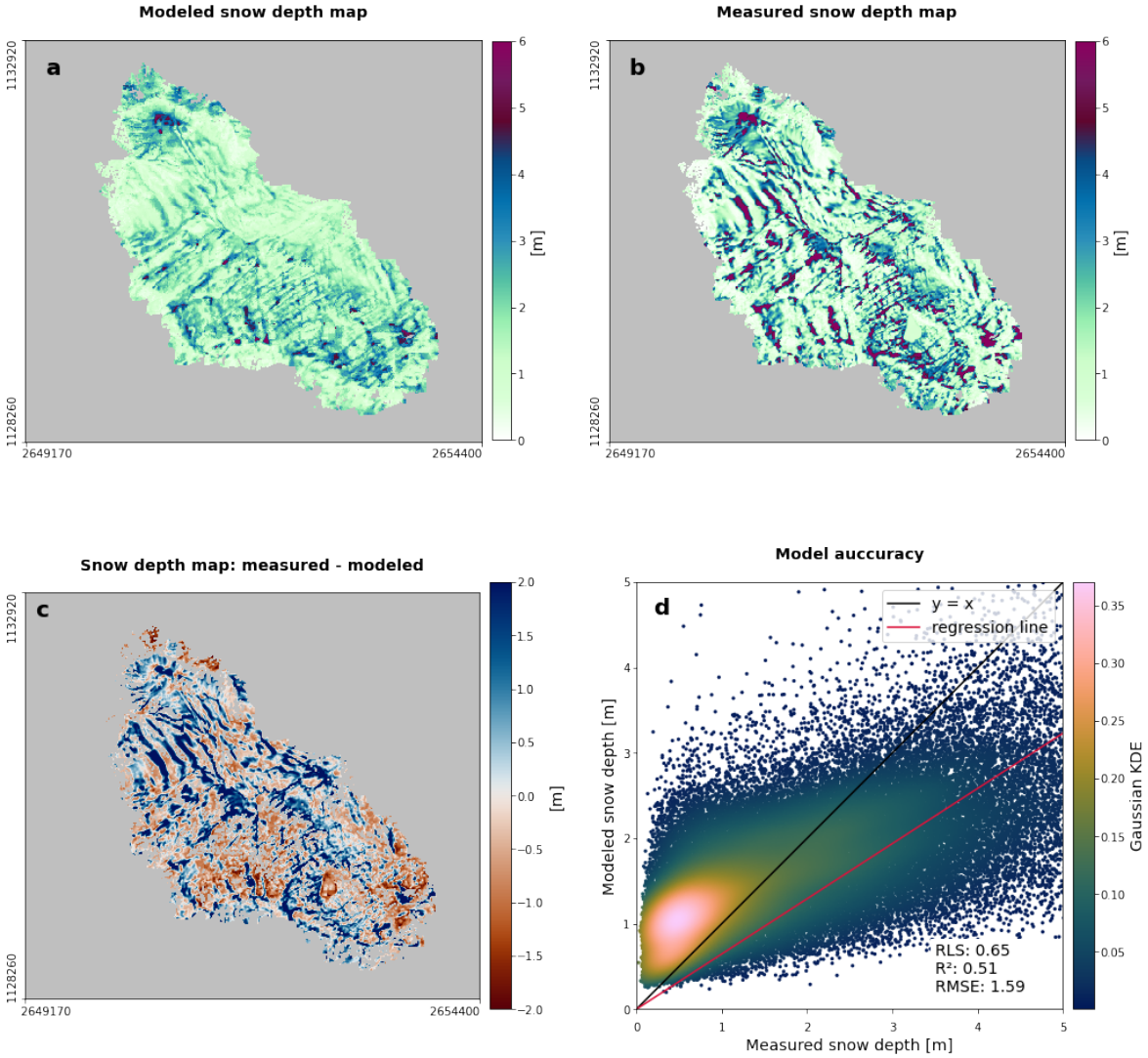

FIGURE C.1: For all plots, the model was trained exclusively with data from the Davos region. (a) modeled snow depth distribution of the Saflischpass at the 23.02.2022. (b) reference snow depth map used for model precision (c) difference between the measured snow depth an the modeled snow depth (d) snow depths model precision. The position of the points (d) depend on the measured snow depth of a pixel (x-axis) and the modeled snow depth at the same pixel (y-axis). The black one-to-one line shows the modeled and measured snow depths coincide. The red regression line shows the optimal correlation of the point cloud. The Regression Line Slope (RSL), coefficient of determination (R^2) and Root Mean Square Error (RMSE) are three statistical values to describe the model precision. The color of the point cloud corresponds to the kernel density estimation and shows the density of the point clouds.

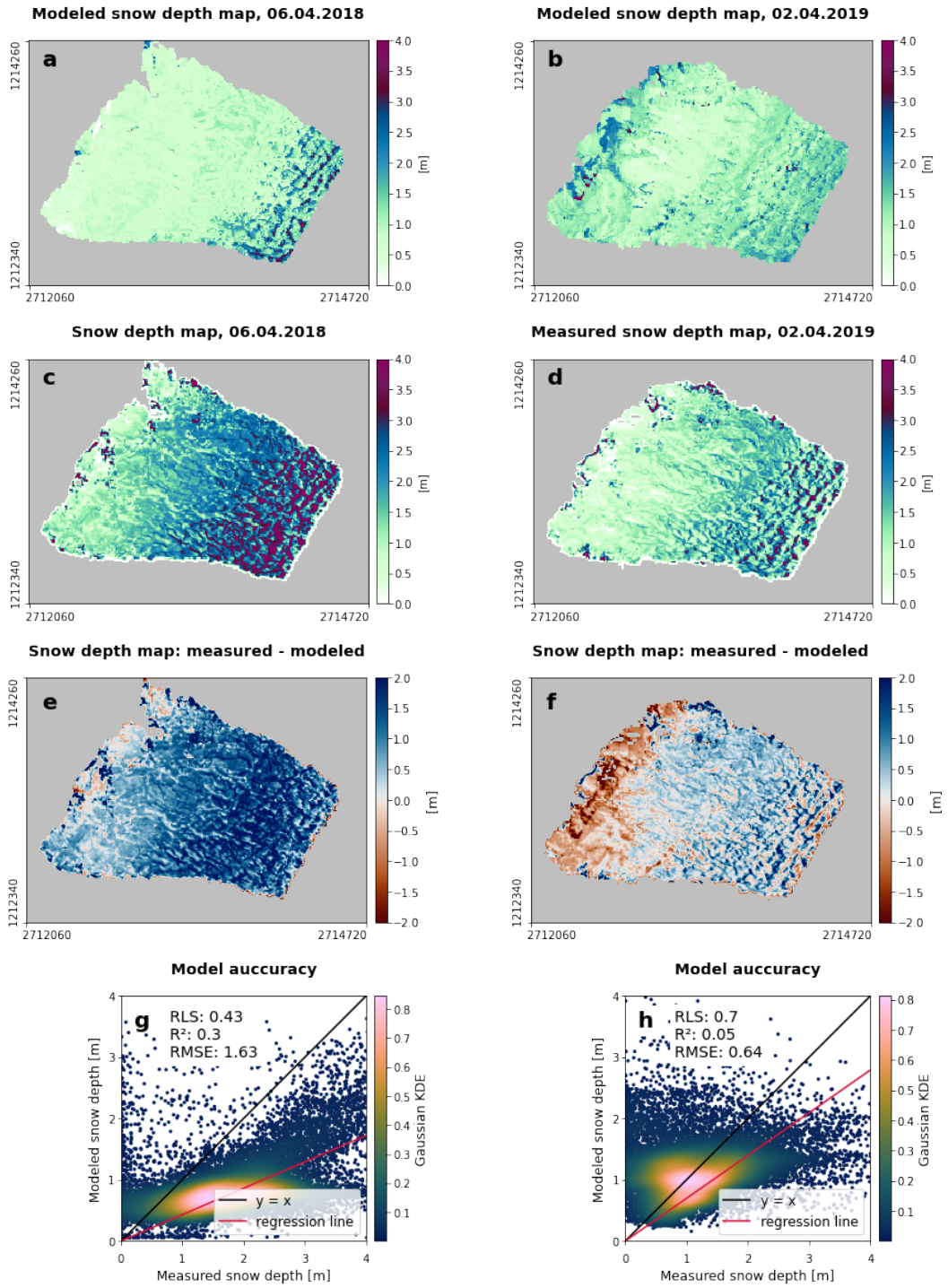

FIGURE C.2: For all plots, the model was trained exclusively with data from the Davos region. (a and b) modeled snow depth distribution of the Wägital at the 06.04.2018 and 02.04.2019 (c and d) reference snow depth map used for model precision (e) difference between the measured snow depth an the modeled snow depth from the 06.04.2018 and (f) from the 02.04.2019 (g) snow depths model precision from the 06.04.2018 (h) snow depths model precision from the 02.04.2019. The position of the points (g and h) depend on the measured snow depth of a pixel (x-axis) and the modeled snow depth at the same pixel (y-axis). The black one-to-one line shows the modeled and measured snow depths coincide. The red regression line shows the optimal correlation of the point cloud. The Regression Line Slope (RSL), coefficient of determination (R^2) and Root Mean Square Error (RMSE) are three statistical values to describe the model precision. The color of the point cloud corresponds to the kernel density estimation and shows the density of the point clouds.

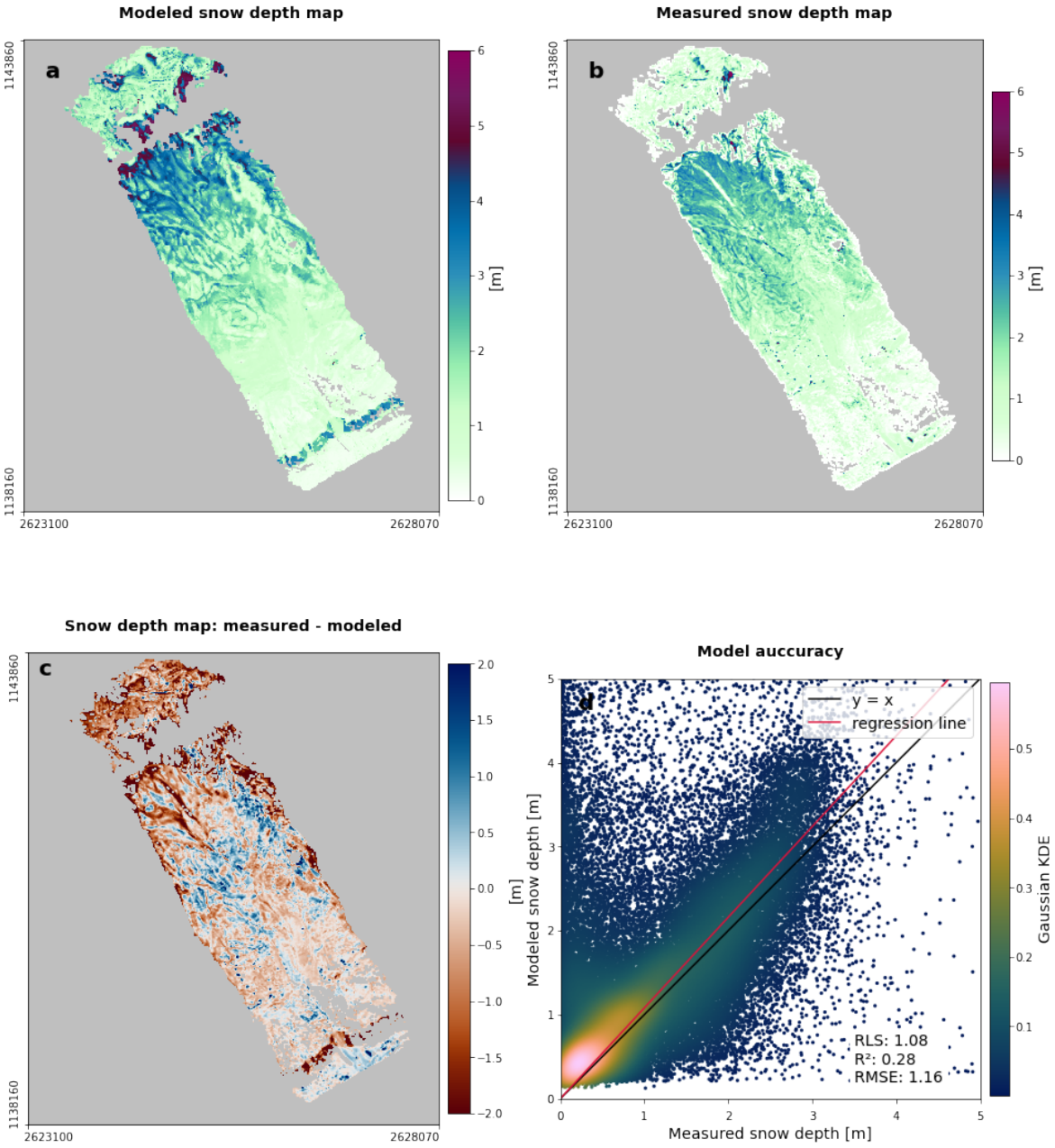

FIGURE C.3: For all plots, the model was trained exclusively with data from the Davos region. (a) modeled snow depth distribution of the Laucherenalp at the 24.02.2022. (b) reference snow depth map used for model precision (c) difference between the measured snow depth an the modeled snow depth (d) snow depths model precision. The position of the points (d) depend on the measured snow depth of a pixel (x-axis) and the modeled snow depth at the same pixel (y-axis). The black one-to-one line shows the modeled and measured snow depths coincide. The red regression line shows the optimal correlation of the point cloud. The Regression Line Slope (RSL), coefficient of determination (R^2) and Root Mean Square Error (RMSE) are three statistical values to describe the model precision. The color of the point cloud corresponds to the kernel density estimation and shows the density of the point clouds.

Acknowledgements

I would like to thank my supervisor Dr. Hendrik Wulf from University of Zurich for his close support during the whole work. I learned a lot from many discussions and scientific advice. I was able to use his data on snow cover duration, which improved the model considerably. For topics requiring additional discussion, Hendrik referred me to various experts.

A big thanks to my co-supervisor Dr. Yves Bühler from the SLF for sharing the snow data and answering my question about snow processes.

Also thanks to Prof. Dr. Alexander Damm from the University of Zurich for his support.

I would also like to thank Bernhard Sassik from the ExoLab for the interpolated snow depths of the measurement stations, which he preprocessed for me.

Many thanks to Dr. Jesús Revuelto and Paul Billecocq for the open discussion. By generously sharing their snow model, I was able to built my thesis based on their experience and discussed my results with them.

Finally, I thank my family and friends for their support and paciest, especially my sister Manuela and my friend Valerie for proofreading this thesis.

Personal Declaration

I hereby declare that the submitted thesis is the result of my own, independent work. All external sources are explicitly acknowledged in the thesis.

Date
January 31, 2023

Signature
Elena Köpfli